example, the optimal cell number for achieving IVD regeneration from MSC transplantation have not been elucidated. Using a canine model of disc degeneration, the present study examined the dosage of autologous MSCs to transplant, investigated the inhibitory effects of the MSC transplant on disc degeneration, and determined the viability of transplanted MSCs.

MATERIALS AND METHODS

Animal experiments were carried out with IACUC approval. A total of 30 beagle dogs, 12- to 18-month old, weighing approximately 10 kg, (Nosan Beagle; Nosan Corporation, Kanagawa, Japan) were divided equally into five groups of six. The N group was the unoperated control group. Three groups with induced disc degeneration were given subsequent MSC transplants of 10^5, 10^6, or 10^7 cells per disc. The D group of operated controls had induction of disc degeneration without MSC transplants. Lateral radiographs and magnetic resonance imaging (MRI) were obtained for every animal before experimental use to confirm the absence of abnormalities. At 12 weeks after the first operation, final radiological and MRI assessments were obtained and all dogs were euthanized by a lethal dose of 120 mg/kg sodium pentobarbital (Abbott Laboratories, Abbott Park, IL). The L3/4, L4/5, and L5/6 discs were isolated with the vertebral bodies attached.

Disc Degeneration Model

Four weeks before the initial MSC transplantation, disc degeneration was induced in L3/4, L4/5, and L5/6 IVDs by NP aspiration according to the method of Hiyama et al.[18] Briefly, an 18-gauge needle was inserted at the center of the disc through the AF into the NP. To induce disc degeneration, the NP was aspirated using a 10-ml syringe, as previously described. The mean mass of the nucleus pulposus aspirated from each disc was 13.4 ± 4.7 mg.

Bone Marrow Collection, Analyses, and Transplantation of MSCs

Autologous MSCs were obtained from the iliac crest from each animal receiving autologous transplants according to the method of Hiyama et al.[18] To measure survival rate of MSCs transplanted into the NP cavity, the MSCs were infected with AcGFP1 (Takara, Japan), a retrovirus vector expressing the green fluorescent protein (GFP) gene (conditioning studies were performed, data not shown). Vector incorporation was more than 90% (data not shown) using FACS analysis. Following the second passage in culture, adherent autologous MSCs were enzymatically released from monolayer culture and the designated cell number was transplanted percutaneously into IVDs in which degeneration had been induced (L3/4, L4/5, and L5/6) 4 weeks before. Transplants were done in the three lumbar discs in a randomized sequence using a discogram needle (25-gauge) guided by fluoroscopic imaging.

EVALUATIONS

Radiological Assessment

Lateral radiographs were taken under general inhalation anesthesia in all groups at 0, 4, 8, and 12 weeks after induction of degeneration. A fluoroscopic imaging intensifier (70 kV, 10 mA, distance 100 cm) was used. Vertebral body heights and disc heights were measured using image J software (Free soft, Image Processing and Analysis, rsb.info.nih.gov/ijl). The data were then transferred to the Excel software program (Microsoft Excel, 2003) and the disc height index (DHI) was calculated, using the method of Masuda et al.[25] Changes in the DHI were expressed as %DHI and normalized to the measured preoperative IVD height by the following equation [DHI = (post-operative DHI/preoperative DHI) × 100].

MRI Assessment

MRI images were also taken to evaluate signal changes in T2-weighted images at 0, 4, 8, and 12 weeks after the first operation in all groups. All MRIs were obtained using a spine coil (1.5T, Gyroscan, ACS-NT, Powertrak6000, Philips, Amsterdam, the Netherlands) under anesthesia. T2-weighted sections in the sagittal plane were obtained using a fast spin echo sequence with time-to-repetition (TR) of 4,000 ms and time-to-echo (TE) of 150 ms; interslice gap of 0.3 mm; matrix at 512 × 512; the field-of-view (FOV) was 200 mm × 200 mm; the number of excitations was 4 and TSE echo spacing was at 18.8. At 12 weeks after the induction of degeneration, the signal intensity of the T2-weighted image of each disc was evaluated using the Pfirmann classification.[26,27]

Gross Anatomical Findings

The spinal segments from five dogs from each group ($n = 25$ IVDs) were fixed in 10% formalin neutral buffer solution (Wako, Osaka, Japan) and decalcified in Plank–Rychlo solution (Decalcifying Solution A; Wako, Tokyo, Japan). Specimens were cut longitudinally through the center of the disc for macroscopic evaluation.

Histological Examination

Discs L3/4, L4/ 5, and L5/6 were excised from the lumbar spine of 10 dogs from each group ($n = 50$ IVDs). Each IVD was fixed in 10% formalin, decalcified, and embedded in paraffin. The paraffin blocks were stained with hematoxylin and eosin or Safranin-O, and evaluated by histology and immunostaining. The hematoxylin and eosin stain evaluated degenerative changes in annulus fibrosus using the disc degeneration grading system of Nishimura and Mochida.[28] Two observers familiar with human and animal IVD specimens and blinded to this study evaluated the sections. The intraobserver error was very small. The kappa value for grading scale was 0.90, showing an excellent agreement. For immunohistochemistry, primary mouse monoclonal antibody (collagen type II, Daiichi Fine Chemical Co., Toyama, Japan) was used with standard protocol.

Apoptotic Cell Counts

The DeadEnd™ Colorimetric TUNEL System (Promega, Madison, WI) was used according to the manufacturer's instructions to detect apoptotic cells in the NP. End labeling was performed on formalin-fixed sections from lumbar spine of five dogs from MSC-transplantation groups. Positive control sections were pretreated with DNase I (Promega). The terminal deoxynucleotidyl transferase (TdT) was replaced by

PBS for the negative controls. Two pathologists counted the cells in the nucleus pulposus area in 10 random high power fields (HPFs; magnification ×400). The percent of TUNEL positive cells of the total nucleus pulposus cells was calculated.

Viability of Nucleus Pulposus Cells after Transplantation

The viability of cells recovered from nucleus pulposus samples of five dogs from each group ($n = 25$ IVDs) were analyzed at 12 weeks after induction of IVD degeneration. Specimens were weighed, then digested in Dulbecco's modified Eagle medium (DMEM; Gibco, Invitrogen Corporation, Carlsbad, CA) containing 0.4% (w/v) actinase E (Kaken Pharmaceutical Inc., Tokyo, Japan) for 1 h, followed by 2 h in DMEM containing 0.016% (w/v) bacterial collagenase P (Roche Diagnostics GmbH, Mannheim, Germany). The digested tissue was passed through a 70 μm pore size cell filter (Becton Dickinson Labware Co. Ltd, Franklin Lakes, NJ). Cells were washed, filtered (Falcon cell strainer, 100 μm), seeded in 96-well microtiter plates (100 μl, 20,000 cells/well, four-wells/disc), and incubated for 20 min to allow settling. Then, 50 μl of ethidium homodimer-1 (EthD-1, 2 μmol/L)/calcein AM (1.6 μmol/L) solution (Live/Dead® cell viability kit; Invitrogen, Basel, Switzerland) were added to each well and incubated for 20 min. Methanol-treated cells (100 μl/150 μl cell suspension) were used as negative controls. Cell fluorescence was observed using an inverse microscope (Leica, DM IL; filters: I3 S 450–490 nm and N2.1 S 515–560 nm). High-resolution digital photos of three visual fields/well were taken using both filters at 25×. Image analysis software (Quantity One®; Bio-Rad, Hercules, CA) was used to quantify cell numbers.

Evaluation of the Survival of Transplanted MSCs

Formalin-fixed sections from lumbar spine of five dogs from the GFP-positive MSC-transplantation group ($n = 15$ IVDs) were analyzed at 12 weeks after induction of IVD degeneration. At 12 weeks post-degeneration induction were embedded in paraffin blocks and sectioned at about 2 μm. Standard procedures were applied for fluorescent immunohistochemistry with primary antibody (Anti-Green Fluorescent Protein; 1:50; Medical&Biological Laboratories, Nagoya, Japan). Alexa 488 (1:100; Molecular Probes, Eugene, OR) was used as a second antibody. Tissues were mounted on slides using VECTASHIELD Mounting medium with 4′,6′-diamino-2-phenylindole (DAPI) (Vector Laboratories, Burlingame, CA). Two pathologists counted the cells in the nucleus pulposus area in 10 random HPFs (magnification ×400). The percent of GFP-positive MSCs of the total nucleus pulposus cells was calculated.

Statistical Analysis

The significance of differences among means of data on radiograph measurements, TUNEL staining for apoptotic cell counts, Live/Dead® for viability of nucleus pulposus cells after transplantation, and the survival rate of the GFP-positive transplanted MSCs was performed using a repeated measure ANOVA and Fisher's PLSD post hoc test. Statistical significance was accepted at $p < 0.05$. The Kruskal–Wallis test and Mann–Whitney U-test were used to analyze the non-parametric data from MRI and histology grading. The Statview program was used for the statistical analyses. Error bars were set to represent 1 SD unit.

RESULTS

Radiographic and MRI Findings

Radiographs showed significant ($p < 0.01$) narrowing of the disc space at 4 weeks after induction of IVD degeneration in the operated control D group and the MSCs transplant groups. The mean %DHI in the D group continued to decrease until 8 weeks post-induction, then plateaued. The mean %DHI of the N group was nearly 100% throughout the study. In contrast, at 4, 8, and 12 weeks after MSC transplantation the mean %DHI of the MSC-transplanted disc groups was higher than the pre-transplant index. At 4, 8, and 12 weeks after the first operation, the mean %DHI increased significantly ($p < 0.01$) in the transplant groups compared to the D group. No significant differences were seen among the three MSC-transplant groups (Fig. 1). At 12 weeks post-induction, the results of MRI (T2-weighted) signal intensity measurement of discs from the D group was less than all other groups. The MSC-transplant groups showed a significant increase in the disc signal intensity. The use of Pfirrmann's classification revealed a significant delay in the progression of disc degeneration in the transplant groups, suggesting an increase in water content in MSC-transplanted discs.[27] The signal intensity level of the N group was constant throughout the study period. Again, no significant differences were detected among the three MSC-transplant groups (Fig. 2).

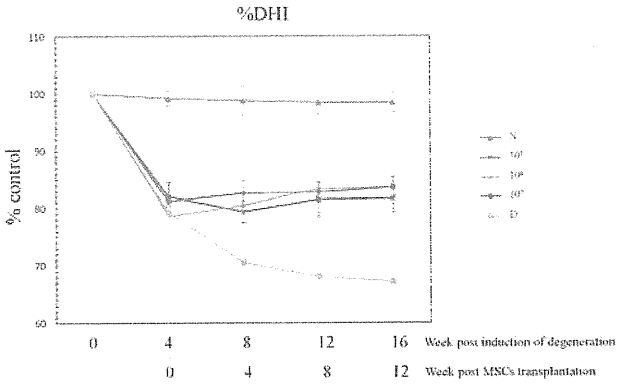

Figure 1. Radiological assessment of mesenchymal stem cell (MSC) transplantation using a canine disc degeneration model. Changes in average %DHI and reductions in %DHI 4 weeks after transplantation of 10^5, 10^6, or 10^7 MSCs. All transplant groups showed significantly ($p < 0.01$) smaller changes than the operated control (D) group (N: 4 w, 98.8 ± 2.5%; 8 w, 98.5 ± 2.1%; 12 w, 98.5 ± 1.7%. 10^7: 4 w, 82.6 ± 2.3%; 8 w, 82.8 ± 1.7%, 12 w, 83.7 ± 1.8%. 10^6: 4 w, 80.5 ± 0.7%; 8 w, 83.4 ± 2.0%, 12 w, 83.7 ± 1.9%. 10^5: 4 w, 79.4 ± 1.9%; 8 w, 81.5 ± 3.0%, 12 w, 81.7 ± 2.4%. D: 4 w, 70.5 ± 1.9%; 8 w, 68.1 ± 2.1%, 12 w, 67.2 ± 3.0%.). No significant differences were seen among the MSC-transplanted groups.

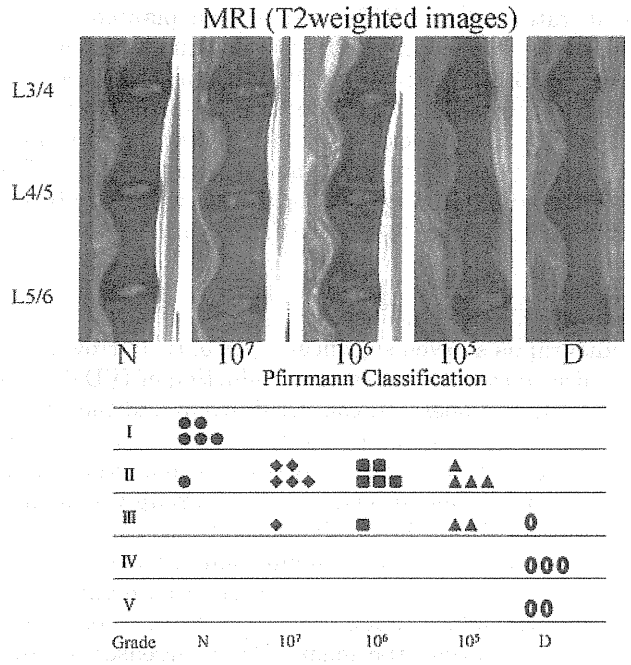

Figure 2. MRI analysis signal changes in T2-weighted images at 12 weeks after induction of degeneration, using the Pfirrmann classification grades 1–5 based on changes in the degree and area of signal intensity. Changes in MRI signal intensity over time showing the signal intensity of the nucleus pulposus was lower ($p < 0.01$) at 12 weeks after transplantation for the operated control D group, but was relatively well maintained for the MSCs transplant groups. No significant differences existed among the three MSCs transplantation groups (N: 1.16 ± 0.4; 10^7: 2.16 ± 0.4; 10^6: 2.16 ± 0.4; 10^5: 2.33 ± 0.5; D: 4.16 ± 0.7).

Macroscopic Findings

The gross appearance of the dissected spines at 12 weeks post-induction of degeneration showed more apparent disc space narrowing and connective tissue invasion of the nucleus cavity in the D group than the other groups. The 10^6 and 10^7 MSC-transplant groups appeared similar to the N group, but the discs from the 10^5 cell transplant group appeared more similar to the connective tissue invasion seen in the D group. Overall, the disc structure was maintained better in the 10^6 and 10^7 cell transplant discs (Fig. 3).

Histology

The histological analysis also showed noteworthy regenerative effects of the MSC transplants. Hematoxylin and eosin staining of N group discs showed a relatively well preserved oval-shaped nucleus with no collapse of inner and outer annular structures. The 10^6 and 10^7 cell groups also showed a relatively well preserved inner annulus structure similar to the N group, but discs from the 10^5 cell group had less preservation of the annular structure (Fig. 4a,c). Safranin-O staining of NPs from the 10^6 and 10^7 groups showed relatively dark staining of nucleus tissue, similar to the N group, while discs from the 10^5 and D groups showed lighter staining of the nucleus and inner annulus (Fig. 4b). The D group stained poorly for collagen type II compared with the other groups (Fig. 5).

Detection of Apoptosis in MSC-Transplanted Discs

The results of TUNEL staining revealed that N group discs had low numbers of apoptotic cells, while D group discs showed significantly higher numbers ($p < 0.01$) of dying and dead cells compared to the other groups. Among the three MSC-transplant groups, the ratio of apoptotic cells was significantly lower for the 10^6 group than the 10^5 and 10^7 groups. No significant difference existed between 10^5 and 10^7 groups ($p = 0.25$; Fig. 6a). There was not a specific region for TUNEL positive cells. It stained scattered in the NP cavity (Fig. 6b).

Assessment of Viability of Nucleus Pulposus Cells after MSC Transplantation

The dual-fluorescence Live/Dead® cell viability assay was used to label viable nucleus pulposus cells 16 weeks after induction of degeneration in the D and MSC-transplant groups. Live cells were stained green with Calcein-AM and dead cells were stained red with Ethidium homodimer-1. The N group had more live cells, while the D group showed significantly ($p < 0.01$) less than the other groups. Among the three MSC-transplant groups, the number of live cells in the 10^6 and 10^7 groups was significantly ($p < 0.01$) greater than the 10^5 group. The 10^7 group had smaller number of live cells than the 10^6 group, although the difference was not statistically significant ($p = 0.20$; Fig. 7).

Survival of Transplanted MSCs in the Nucleus Pulposus

GFP-positive MSCs were detected using an FITC filter. GFP-positive MSCs were seen primarily in the central region of the nucleus pulposus. Only cells that stained with DAPI to show a clearly visible nucleus were counted. These cells were consecutively counted

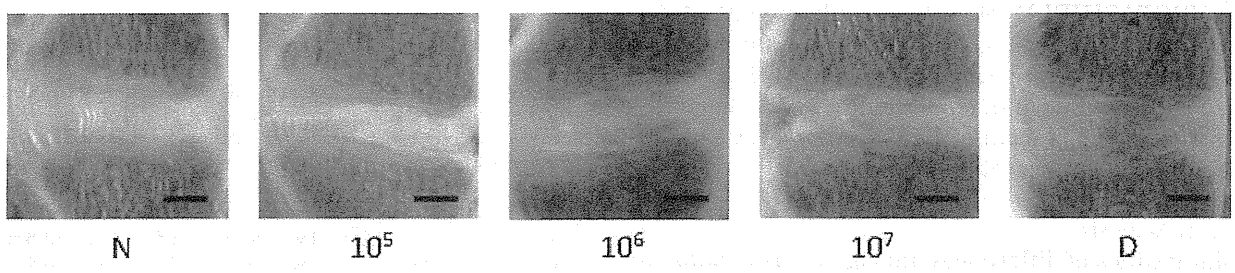

Figure 3. Gross anatomical findings greater intervertebral disc degeneration was seen at 12 weeks after transplantation for the operated control D group when compared to the other groups. Among the transplant groups, the morphology of the MSC 10^6 and 10^7 groups resemble that of the N group, while fewer and less severe morphological changes were seen in 10^5 group. Bar = 5 mm.

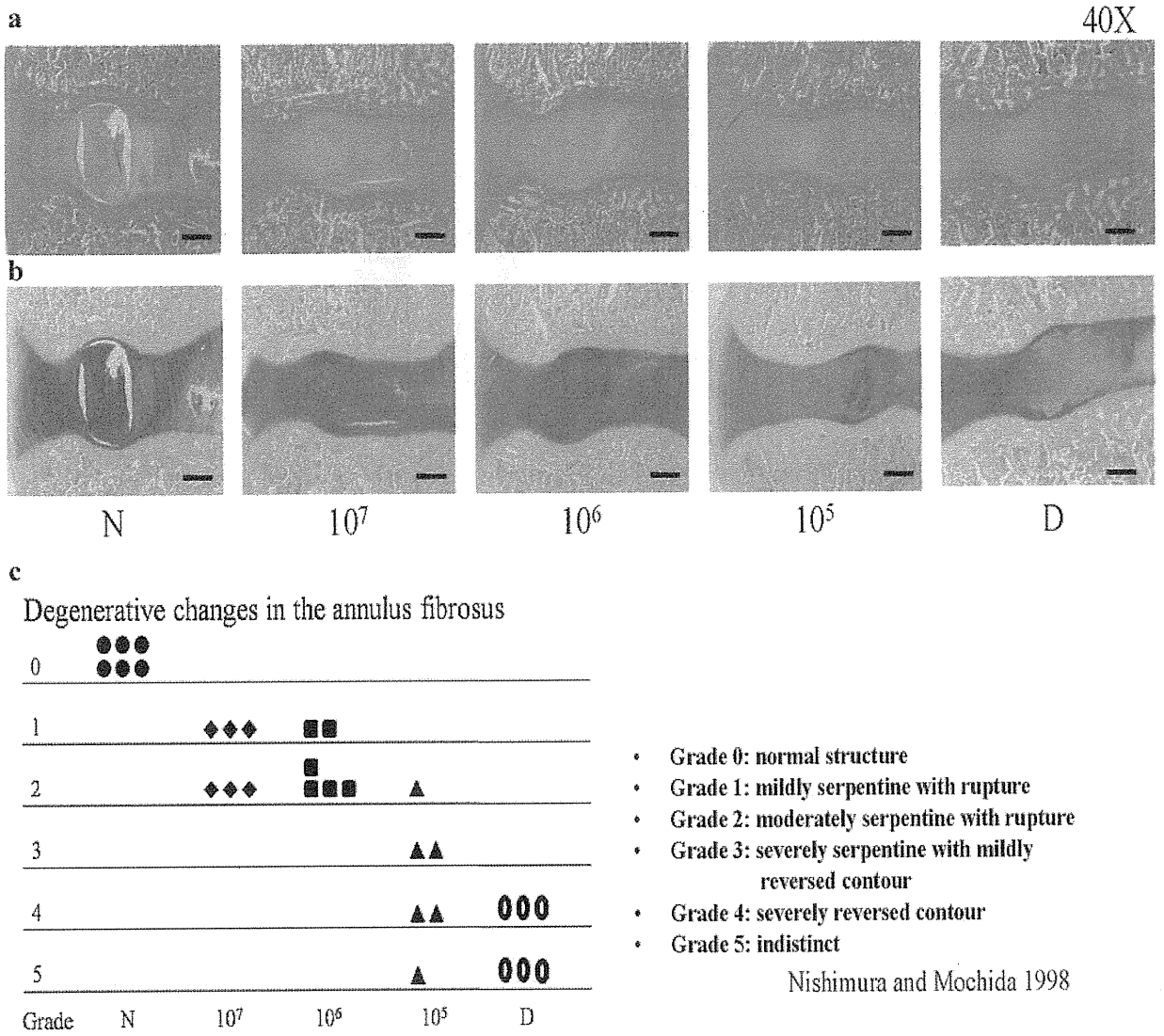

Figure 4. Histology. (a) The structures of degenerative discs receiving mesenchymal stem cell (MSC) transplantation at MSC 10^6 and MSC 10^7 are near normal, but partial disruption of the annulus fibrosus is seen in discs from the 10^5 group. (Hematoxylin and eosin staining, original magnification ×40). (b) Safranin-O staining is stronger in the transplantation group discs compared to the D group. (Original magnification ×40). (c) Histological analysis using the disc degeneration grading system of Nishimura and Mochida, which measures morphological changes in the annular structure, 12 weeks after induction of degeneration, annular structures were significantly ($p < 0.01$) better maintained in the transplant groups than group D (Mann–Whitney test). Bar = 500 μm.

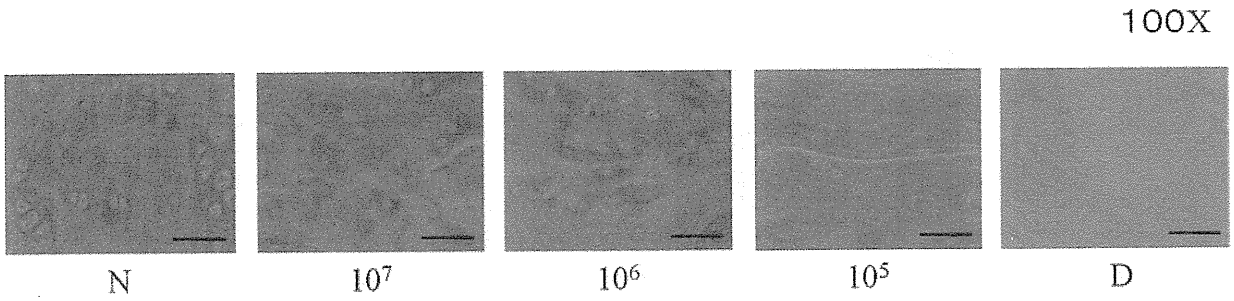

Figure 5. Immunohistochemical staining. Staining of the nucleus pulposus for collagen type II for the operated control D group was weaker than for the other groups. (Original magnification ×100). Bar = 100 μm.

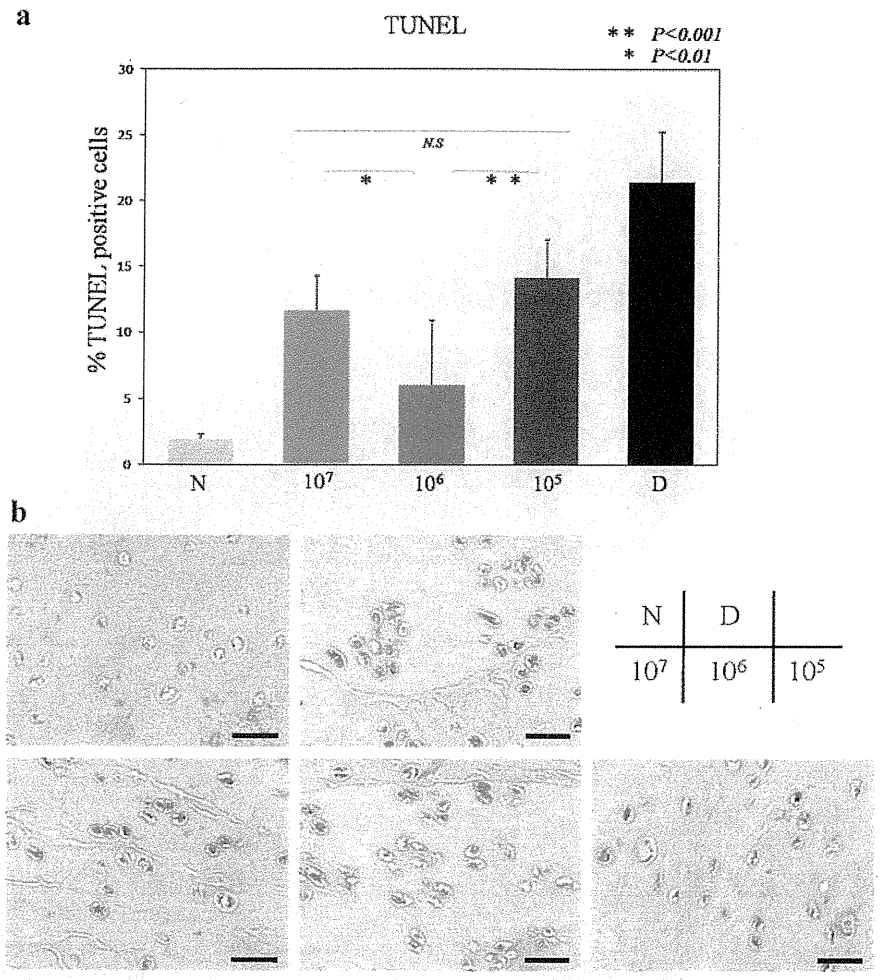

Figure 6. TUNEL staining. (a)The TUNEL staining revealed the N group discs did not show relevant number of apoptotic cells, while the D group discs showed significant increase compared to the other groups. Among the three MSCs transplanted groups, compared to the 10^5 and 10^7 groups, the ratio of apoptotic cells was significantly lower for the 10^6 group. No significant difference existed between 10^5 and 10^7 groups (N: $1.9 \pm 0.4\%$; 10^7: $11.7 \pm 2.6\%$; 10^6: $6.0 \pm 4.9\%$; 10^5: $14.2 \pm 2.9\%$; D: $21.5 \pm 3.8\%$; $p = 0.25$). (b) TUNEL staining of the NP cavity formed at 12 weeks after first operation. Bar = 100 μm.

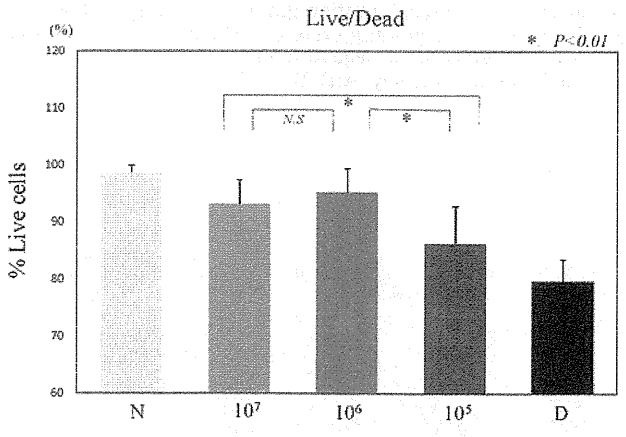

Figure 7. LIVE/DEAD cell viability assay. The LIVE/DEAD assay of vertebral tissues 12 weeks after transplantation shows that the number of living NP cells in the 10^6 and 10^7 groups was significantly ($^*p < 0.01$) higher than that of the 10^5 group (N: $98.1 \pm 1.1\%$; 10^7: $91.7 \pm 2.4\%$; 10^6: $94.5 \pm 3.5\%$; 10^5: $85.7 \pm 5.8\%$; D: $79.4 \pm 3.4\%$).

in 10 randomly selected visual fields of nucleus pulposus area and averaged after costaining with GFP to detect the labeled transplanted MSCs. Percentages of GFP-positive cells for the 10^6 cell group was 62.8 ± 12.4, and the 10^7 group $75.2 \pm 16.1\%$, both were significantly ($p < 0.01$) higher than the $15.3 \pm 9.2\%$ found in the 10^5 group (Fig. 8a). There was no specific region for its distribution and they were scattered in NP cavity (Fig. 8b).

DISCUSSION

In order to evaluate the effect of cell doses in MSCs transplantation for experimental disc degeneration, changes in disc height, as assessed by radiographic %DHI, signal, and in relative signal intensity as classified by Pfirrman et al. of the nucleus pulposus on MRI T2-weighted imaging were determined. We found that the increase of %DHI in the MSC-transplant groups compared to the D group decreased beginning at 4 weeks after transplantation. On T2-weighted imaging, MSCs transplanted discs showed less degeneration

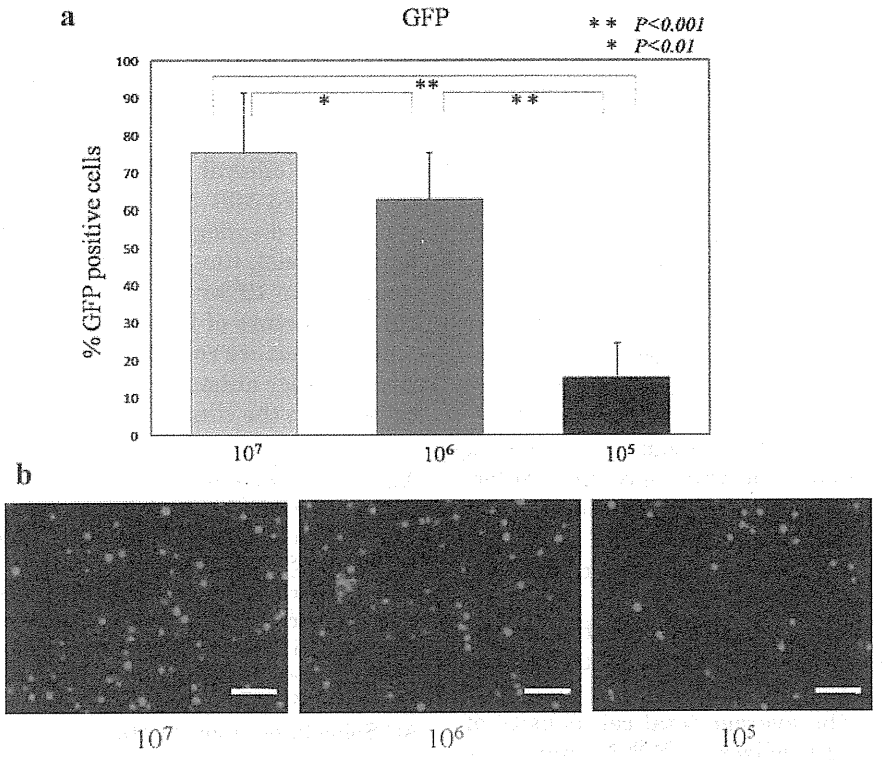

Figure 8. Green fluorescent protein (GFP) positive cells. (a) The number of GFP-positive MSCs in the nucleus pulposus at 12 weeks after transplantation was significantly (**$p < 0.001$) higher for the 10^6 and 10^7 groups than for the 10^5 group. (b) GFP-positive cells image of the NP cavity formed at 12 weeks after first operation. Bar = 100 μm.

in Pfirrman classification. Diagnostic imaging results showed that the progression of IVD degeneration was inhibited in all three MSC-transplanted groups, with no significant differences among the three groups. Evaluation of the histology of the experimental discs indicated that disc degeneration was limited in the MSC-transplant groups. The annulus fibrosus structures were maintained at near normal status in the MSC 10^6 and 10^7 groups, but not the 10^5 group. In the NP of the MSC 10^6 and 10^7 groups, proteoglycan, type II collagen, and other extracellular matrix components were maintained, indicating that IVD degeneration was suppressed. There were no significant differences in imaging results between 10^5 versus 10^6 and 10^7 groups in MSC-transplanted group discs despite the fact that there were significant differences in histological analysis. This may be resulting from the fact that disc height and T2-weighted signal on MRI would not correlate directly to histological disc degeneration in short observation time. In the previous literature, Ho et al.[22] suggested that differences between imaging and histological findings are probably due to differences in sensitivity between diagnostic imaging and histological analysis; however, differences in follow-up time intervals may also contribute. Further studies utilizing longer follow-up times are needed to resolve the differences between imaging and histological findings.

The three parameters used to assess post-transplant cell activity in discs were the number of remaining transplanted MSCs, the survival rate of NP cells, and apoptosis of NP cells in transplanted discs. For the MSC 10^5 group, the numbers of transplanted MSCs remaining and viable cells in the nucleus pulposus tissue were low. An insufficient cell number may not be capable of reconstructing the matrix and microenvironment of degenerating discs, resulting in increased death of both resident and transplanted cells. As seen in the MSC 10^7 group, when too many cells were transplanted into the limited space of the IVD, an imbalance between the relatively slow rate of diffusion of nutrients and cell number may have occurred, inducing apoptosis of both transplanted MSCs and resident cells; this needs to be verified in longer-term studies. These findings from the transplantation of 10^5, 10^6, and 10^7 MSCs suggest that quantity of the transplanted cells are important to optimize the inhibition of progression of degeneration and to regenerate damaged IVDs and that there most likely is a minimal number that affects its therapeutic effect. However, there is still much more parameters to discuss such as evaluation of adequate nutrition for the number of MSCs transplanted which may also be important for maintaining the microenvironment of the disc or differentiation status of the transplanted MSCs. Inducing MSCs towards NP in vitro may most likely affect the therapeutic outcome as well.

Animal models for studies of cell transplantation in IVD degeneration have employed rabbits, rats, and larger animals, such as beagles.[23,24,29] Several techniques have been developed to produce disc degeneration, but an ideal animal model for the human

condition has not been established.[30–32] It has been well known that notochord-like cells are present in the nucleus pulposus of rats and young rabbits, whereas only chondrocyte-like cells constitute the nucleus pulposus in humans. Small animals may therefore be unsuitable for use as models of the human disease. We use beagles as an alternative animal model because we believe the discs of this chondrodystrophic breed more closely approximate the anatomy of human discs. In addition, beagle IVD degeneration and herniation are likely to occur spontaneously, and beagle nucleus pulposus cells are chondrocyte-like. Beagles are sometimes being used to study IVD degeneration since their disc cells share similarities with human discs.[33–37]. Degeneration is produced by nucleotomy in the model used in the present study, and thus may have differences from naturally occurring IVD degeneration in humans. Although this may be considered a limitation of this model, no animal model that completely mimics human IVD degeneration exists at this time. The nucleotomy model may well have usefulness for studying disc degeneration progression following disc surgery.

In the human NP, the average total cell density of the disc is about $4–6 \times 10^3$ cells/mm^3.[38,39] Human discs are rich in extracellular matrix and possess immune privilege. For clinical application, the optimal number of MSCs transplanted to restore these characteristics in damaged IVDs must be determined. In a supplementary experiment, we investigated 20 IVD specimens from 10 beagles, 10 of which were normal IVDs taken from beagles sacrificed at a very similar age and from the same disc level of animals used in the study and 10 of which same procedure was performed as the initial study for induction of disc degeneration. Results demonstrated that average volume of NP tissue in single IVDs of beagles used in the study was 107.18 ± 1.03 mg (wet weight) and the average viable cell number was $1.03 \pm 0.19 \times 10^6$ cells. For the IVDs, where induction of disc degeneration was performed, average volume of NP tissue at the time of injection was 87.38 ± 4.23 mg (wet weight) and the average viable cell number was $1.36 \pm 0.15 \times 10^5$ cells. These data indicates that there is not truly a large difference in number of viable cells among the IVDs used in the study. This also justifies the rational of injecting equal numbers of MSCs in the discs. Furthermore, a base line of 10^6 viable cells may be the adequate number to maintain disc homeostasis, which also is understandable in interpreting the result of initial study where injection of 10^5 cells was not fully sufficient. Previous animal model studies of cell transplantation to IVDs have used 10^6 cells/disc for transplants,[15–18] therefore, we transplanted 10^5, 10^6, or 10^7 cells per disc in the present study, establishing three transplant groups with the number of cells transplanted increasing at 10- to 100-fold. Although actual clinical situation for translation of this procedure will not be clarified without clinical trials, we believe that grade 2 or 3 in Pfirrman classification, where disc degeneration is mild-to-moderate with less nutritional problem may be one candidate.[40]

In the present study, the effect of the number of MSCs transplanted into a degenerative disc was investigated using a canine disc degeneration model. From the perspective of clinical application, the optimal number of transplanted cells may also be affected by the severity of recipient disc degeneration.[22] However, in the current limited model, the transplantation of 10^6 MSCs, when compared to 10^5 or 10^7, produced the best maintenance of the structure of IVDs and best inhibited IVD degeneration. Because results from a study such as ours may vary in other animal models and in humans, care must be taken in the clinical application of our findings.

ACKNOWLEDGMENTS

The authors would like to thank Tomoko Nakai and Sachie Tanaka and Teaching and Research Support Center at Tokai University School of Medicine for their technical assistance. This work was supported in part by a Grant-in-Aid for Scientific Research and a Grant of The Science Frontier Program from the Ministry of Education, Culture, Sports, Science and Technology of Japan D.S. and J.M., a grant from 2008 Tokai University School of Medicine Research Aid and a grant from AO Spine International to D.S.

REFERENCES

1. Andersson GB, Lucente T, Davis AM, et al. 1999. A comparison of osteopathic spinal manipulation with standard care for patients with low back pain. N Engl J Med 341:1426–1431.
2. Borenstein D. 1992. Epidemiology, etiology, diagnostic evaluation, and treatment of low back pain. Curr Opin Rheumatol 4:226–232.
3. Gruber HE, Hanley EN Jr. 2002. Ultrastructure of the human intervertebral disc during aging and degeneration: comparison of surgical and control specimens. Spine 27:798–805.
4. Luoma K, Riihimäki H, Luukkonen R, et al. 2000. Low back pain in relation to lumbar disc degeneration. Spine 25:487–492.
5. Luoma K, Vehmas T, Raininko R, et al. 2004. Lumbosacral transitional vertebra: relation to disc degeneration and low back pain. Spine 29:200–205.
6. Masuda K, An HS. 2004. Growth factors and the intervertebral disc. Spine J 4(Suppl 6)330S–340S.
7. Masuda K, An HS. 2006. Prevention of disc degeneration with growth factors. Eur Spine J 15(Suppl 3):422S–432S.
8. Masuda K, Imai Y, Okuma M, et al. 2006. Osteogenic protein-1 injection into a degenerated disc induces the restoration of disc height and structural changes in the rabbit anular puncture model. Spine 31:742–754.
9. Thompson JP, Oegema TR Jr, Bradford DS. 1991. Stimulation of mature canine intervertebral disc by growth factors. Spine 16:253–260.
10. Walsh AJ, Bradford DS, Lotz JC. 2004. In vivo growth factor treatment of degenerated intervertebral disc. Spine 29:156–163.
11. Paul R, Haydon RC, Cheng H, et al. 2003. Potential use of Sox9 gene therapy for intervertebral degenerative disc disease. Spine 28:755–763.
12. Nishida K, Kang JD, Suh JK, et al. 1998. Adenovirus mediated gene transfer to nucleus pulposus cells. Implications for the treatment of intervertebral disc degeneration. Spine 23:2437–2442.

13. Nishida K, Kang JD, Gilbertson LG, et al. 1999. Modulation of the biologic activity of the rabbit intervertebral disc by gene therapy: an in vivo study of adenovirus-mediated transfer of the human transforming growth factor beta 1 encoding gene. Spine 24:2419–2425.
14. Sato M, Asazuma T, Ishihara M, et al. 2003. An experimental study of the regeneration of the intervertebral disc with an allograft of cultured annulus fibrosus cells using a tissue-engineering method. Spine 28:548–553.
15. Sakai D, Mochida J, Yamamoto Y, et al. 2003. Transplantation of mesenchymal stem cells embedded in Atelocollagen gel to the intervertebral disc: a potential therapeutic model for disc degeneration. Biomaterials 24:3531–3541.
16. Sakai D, Mochida J, Iwashina T, et al. 2005. Differentiation of mesenchymal stem cells transplanted to a rabbit degenerative disc model: potential and limitations for stem cell therapy in disc regeneration. Spine 30:2379–2387.
17. Sakai D, Mochida J, Iwashina T, et al. 2006. Regenerative effects of transplanting mesenchymal stem cells embedded in atelocollagen to the degenerated intervertebral disc. Biomaterials 27:335–345.
18. Hiyama A, Mochida J, Iwashina T, et al. 2008. Transplantation of mesenchymal stem cells in a canine disc degeneration model. J Orthop Res 26:589–600.
19. Okano H. 2002. Stem cell biology of the central nervous system. J Neurosci Res 15:698–707.
20. Caplan AI. 1991. Mesenchymal stem cells. J Orthop Res 9:641–650.
21. Henriksson HB, Svanvik T, Jonsson M, et al. 2009. Transplantation of human mesenchymal stems cells into intervertebral discs in a xenogeneic porcine model. Spine 34:141–148.
22. Ho G, Leung VY, Cheung KM, et al. 2008. Effect of severity of intervertebral disc injury on mesenchymal stem cell-based regeneration. Connect Tissue Res 49:15–21.
23. Nomura T, Mochida J, Okuma M, et al. 2001. Nucleus pulposus allograft retards intervertebral disc degeneration. Clin Orthop 389:94–101.
24. Okuma M, Mochida J, Nishimura K, et al. 2000. Reinsertion of stimulated nucleus pulposus cells retards intervertebral disc degeneration: an in vitro and in vivo experimental study. J Orthop Res 18:988–997.
25. Masuda K, Aota Y, Muehleman C, et al. 2005. A novel rabbit model of mild, reproducible disc degeneration by an anulus needle puncture: correlation between the degree of disc injury and radiological and histological appearances of disc degeneration. Spine 30:5–14.
26. Thompson JP, Pearce RH, Schechter MT, et al. 1990. Preliminary evaluation of a scheme for grading the gross morphology of the human intervertebral disc. Spine 15:411–415.
27. Pfirrmann CW, Metzdorf A, Zanetti M, et al. 2001. Magnetic resonance classification of lumbar intervertebral disc degeneration. Spine 26:1873–1878.
28. Nishimura K, Mochida J. 1998. Percutaneous reinsertion of the nucleus pulposus. An experimental study. Spine 23:1531–1538.
29. Singh K, Masuda K, An HS. 2005. Animal models for human disc degeneration. Spine J 5(Suppl 6):267S–279S.
30. Chujo T, An HS, Akeda K, et al. 2006. Effects of growth differentiation factor-5 on the intervertebral disc—in vitro bovine study and in vivo rabbit disc degeneration model study. Spine 31:2909–2917.
31. Gruber HE, Johnson T, Norton HJ, et al. 2002. The sand rat model for disc degeneration: radiologic characterization of age-related changes: cross-sectional and prospective analyses. Spine 27:230–234.
32. Hutton WC, Yoon ST, Elmer WA, et al. 2002. Effect of tail suspension (or simulated weightlessness) on the lumber intervertebral disc: study of proteoglycans and collagen. Spine 27:1286–1290.
33. Fujita N, Miyamoto T, Imai J, et al. 2005. CD24 is expressed specifically in the nucleus pulposus of intervertebral discs. Biochem Biophys Res Commun 30:1890–1896.
34. Semba K, Araki K, Li Z, et al. 2006. A novel murine gene, sickle tail, linked to the Danforth's short tail locus, is required for normal development of the intervertebral disc. Genetics 172:445–456.
35. Hunter CJ, Matyas JR, Duncan NA. 2004. Cytomorphology of notochordal and chondrocytic cells from the nucleus pulposus: a species comparison. J Anat 205:357–362.
36. Gillett N, Gerlach R, Cassidy JJ, et al. 1988. Age-related changes in the beagle spine. Acta Orthop Scand 59:503–507.
37. Ganey T, Libera J, Moos V, et al. 2003. Disc chondrocyte transplantation in a canine model: a treatment for degenerated or damaged intervertebral disc. Spine 28:2609–2620.
38. Oegema TR Jr. 1993. Biochemistry of the intervertebral disc. Clin Sports Med 12:419–439.
39. Maroudas A, Stockwell RA, Nachemson A, et al. 1975. Factors involved in the nutrition of the human lumbar intervertebral disc: cellularity and diffusion of glucose in vitro. J Anat 120:113–130.
40. Grunhagen T, Wilde G, Soukane DM, et al. 2006. Nutrient supply and intervertebral disc metabolism. J Bone Joint Surg Am 88(Suppl 2):30–35.

ARTHRITIS & RHEUMATISM
Vol. 62, No. 10, October 2010, pp 3036–3047
DOI 10.1002/art.27599

Enhancement of Intervertebral Disc Cell Senescence by WNT/β-Catenin Signaling–Induced Matrix Metalloproteinase Expression

Akihiko Hiyama,[1] Daisuke Sakai,[1] Makarand V. Risbud,[2] Masahiro Tanaka,[1] Fumiyuki Arai,[1] Koichiro Abe,[1] and Joji Mochida[1]

Objective. **To determine whether intervertebral disc (IVD) cells express β-catenin and to assess the role of the WNT/β-catenin signaling pathway in cellular senescence and aggrecan synthesis.**

Methods. **The expression of β-catenin messenger RNA (mRNA) and protein in rat IVD cells was assessed by using several real-time reverse transcription–polymerase chain reaction, Western blot, immunohistochemical, and immunofluorescence analyses. The effect of WNT/β-catenin on nucleus pulposus (NP) cells was examined by transfection experiments, an MTT assay, senescence-associated β-galactosidase staining, a cell cycle analysis, and a transforming growth factor (TGFβ)/bone morphogenetic protein (BMP) pathway–focused microarray analysis.**

Results. **We found that β-catenin mRNA and protein were expressed in discs in vivo and that rat NP cells exhibited increased β-catenin mRNA and protein upon stimulation with lithium chloride, a known activator of WNT signaling. LiCl treatment inhibited the proliferation of NP cells in a time- and dose-dependent manner. In addition, there was an increased level of cellular senescence in LiCl-treated cells. Long-term treatment with LiCl induced cell cycle arrest and promoted subsequent apoptosis in NP cells. Activation of WNT/β-catenin signaling also regulated the expression of aggrecan. We also demonstrated that WNT/β-catenin signaling induced the expression of matrix metalloproteinases (MMPs) and TGFβ in NP cells.**

Conclusion. **The activation of WNT/β-catenin signaling promotes cellular senescence and may modulate MMP and TGFβ signaling in NP cells. We hypothesize that the activation of WNT/β-catenin signaling may lead to an increased breakdown of the matrix, thereby promoting IVD degeneration.**

The intervertebral disc (IVD) allows for movement between adjacent vertebrae and accommodates compressive forces that are applied to the spine. The IVD consists of a peripheral anulus fibrosus (AF) that encloses a gel-like tissue called the nucleus pulposus (NP). The unique water-binding properties of the NP promote dynamic loading and unloading, permitting the spine to experience and contain large shifts in biomechanical forces. Disc degeneration is characterized by desiccation of tissue as a result of loss of cells and breakdown of the extracellular matrix.

In recent years, the rapid progress in medical technology has been striking. The clinical conditions and causal factors of low back pain and related diseases have been characterized in more detail, and new treatments and treatment approaches have been developed (1–8). However, the mechanisms of IVD degeneration resulting in low back pain have not yet been characterized at the molecular level. Many studies have shown an increase in the expression and activity of matrix metalloproteinases (MMPs) during IVD degeneration, and prominent extracellular matrix components of the disc, including types I and II collagen and aggrecan, have

Supported by the Japan Orthopaedics and Traumatology Foundation (grant 0120), the Ministry of Education, Culture, Sports, Science, and Technology of Japan (Grant-in-Aid for Scientific Research and a Science Frontier Program grant), and Tokai University School of Medicine (research grant). Dr. Risbud's work was supported by the NIH (grants R01-AR-050087 and R01-AR-055655).

[1]Akihiko Hiyama, MD, PhD, Daisuke Sakai, MD, PhD, Masahiro Tanaka, MD, Fumiyuki Arai, MD, Koichiro Abe, MD, Joji Mochida, MD: Tokai University School of Medicine, Isehara, Japan; [2]Makarand V. Risbud, PhD: Thomas Jefferson University, Philadelphia, Pennsylvania.

Address correspondence and reprint requests to Akihiko Hiyama, MD, PhD, Department of Orthopaedic Surgery, Surgical Science, Tokai University School of Medicine, Bohseidai, Isehara, Kanagawa 259-1193, Japan. E-mail: a.hiyama@tokai-u.jp.

Submitted for publication February 23, 2010; accepted in revised form June 3, 2010.

been shown to be substrates of various MMPs (9–12). Richardson et al (13) recently showed a correlation between expression of the pain-related factors nerve growth factor and substance P as well as MMP-10 and both the disease severity and the pain severity in patients with disc degeneration (13).

Another important factor in the process of disc degeneration is the decrease in the overall number of matrix-producing cells. Moreover, there is some indication that disc cells undergo enhanced cellular senescence, and there is a decreased ability to undergo proliferation (14). Over the last several years, genes with functions that contribute to the aging process have been identified, and many of these are closely related to elements involved in cellular senescence, such as stress control and DNA repair (15–18). It is therefore possible that cellular senescence may be one cause of individual aging (17,19).

It has been reported that in osteoarthritic articular cartilage, there is increased accumulation of β-catenin and decreased expression of aggrecan and Col2a1 (20). In addition, several groups have reported that the WNT family is involved in regulating a variety of processes during development. For example, recent studies in mouse and chick models have demonstrated that WNT molecules exert negative effects on chondrogenesis (21,22).

WNT signals typically involve a noncanonical pathway or a canonical pathway, and of these, the canonical WNT/β-catenin pathway, which activates the transcription factors T cell factor (TCF) and lymphoid enhancer factor (LEF) through β-catenin activity, is well known (23–27). When the WNT ligand is absent, β-catenin undergoes glycogen synthase kinase 3β (GSK-3β)–mediated phosphorylation and proteasome-mediated degradation. When the WNT ligand is present, it interacts with its receptor, low-density lipoprotein receptor–related protein 5/6, which recruits Axin to facilitate Axin decomposition. In addition, Disheveled facilitates the dissociation of the adenomatous polyposis coli/Axin/GSK-3β complex while FRAT/GBP directly inhibits GSK-3β phosphorylation activity. As a result, the phosphorylation of β-catenin by GSK-3β is inhibited, and the β-catenin is stabilized. The stabilized β-catenin moves into the nucleus and, together with TCF and LEF, controls the formation of the body axis and somites, as well as cellular proliferation and differentiation (28). The quantitative changes of β-catenin are therefore an extremely important factor. However, the role of WNT/β-catenin signals in IVD cells is not yet well understood.

In the present study, we examined the expression and regulatory role of WNT/β-catenin signaling in NP cell function. The present experiments were designed to examine whether the WNT/β-catenin signal controls NP cell differentiation/proliferation and senescence. Our results show that NP cell senescence is regulated by the WNT/β-catenin signaling pathway, and that the WNT/β-catenin signal may play an important role in IVD degeneration through an activated MMP signaling pathway.

MATERIALS AND METHODS

Reagents and plasmids. To determine the β-catenin–TCF/LEF transcription activity, NP cells and AF cells were transiently transfected with the TCF/LEF reporter gene TOPflash (optimal TCF binding site) or FOPflash (mutated TCF binding site) (Upstate Biotechnology). The luciferase reporter plasmids encoding the aggrecan promoter (Agg-Luc) or the type II collagen promoter (Col2-Luc) were provided by Dr. Michael C. Naski (University of Texas Health Science Center at San Antonio). The type II collagen promoter uses the rat type II collagen promoter and enhancer (29). The aggrecan promoter carries 1.2 kb of the proximal mouse promoter (30). MMP-10-Luc was provided by Dr. Rhonda Bassel-Duby (Department of Molecular Biology, University of Texas Southwestern Medical Center at Dallas). MMP-9-Luc was provided by Dr. Douglas D. Boyd (M. D. Anderson Cancer Center, Houston, TX). The WT-β-catenin expression plasmid and the backbone plasmid were provided by Dr. Raymond Poon (Hospital for Sick Children, University of Toronto, Toronto, Ontario, Canada). As an internal transfection control, we used vector pGL4.74 (Promega) containing the *Renilla reniformis* luciferase gene. Lithium, a therapeutic agent in neurodegenerative disorders and a known inducer of β-catenin, was used to treat cells.

Isolation of intervertebral disc cells. A total of 64 female Sprague-Dawley rats (12 weeks old) were used for this study. Rats were euthanized by injection of an excess amount of pentobarbital sodium (100 mg/kg of Nembutal; Abbott Laboratories). The spinal columns were removed under aseptic conditions, and lumbar IVDs were separated. The gel-like NP was separated from the AF. The NP tissue obtained was digested for 30 minutes in a mixture of 0.4% Pronase (Kakenkagaku) and 0.0125% collagenase P (Boehringer Mannheim). The AF tissue was digested for 1 hour with 0.4% Pronase and for 3 hours with 0.025% collagenase P. The digested tissue was passed through a cell strainer (BD Falcon) with a pore size of 100 μm and was washed 2 times with phosphate buffered saline (PBS; Gibco). The isolated cells were maintained in Dulbecco's modified Eagle's medium (DMEM) and 10% fetal bovine serum (FBS) supplemented with antibiotics at 37°C in a humidified atmosphere of 5% CO_2. When confluent, the NP and AF cells were harvested and subcultured in 10-cm dishes. We used the low-passage cells (<3 passages) cultured in a monolayer.

Immunofluorescence microscopy. NP cells were plated in 96-well flat-bottomed plates (5,000 cells/well) and treated

with LiCl (20 m*M*) for 24 hours. After incubation, cells were fixed with 4% paraformaldehyde, permeabilized with 0.2% Triton X-100 in PBS for 10 minutes, blocked with PBS containing 5% FBS, and incubated overnight at 4°C with antibodies against β-catenin (1:200 dilution; Cell Signaling Technology), MMP-9 (1:200 dilution; Santa Cruz Biotechnology), and MMP-10 (1:200 dilution; Santa Cruz Biotechnology). After washing the primary antibodies, the cells were incubated for 1 hour at room temperature with an anti-rabbit Alexa Fluor 488 or an anti-goat Alexa Fluor 594 anti-rabbit secondary antibody (Invitrogen), each at a dilution of 1:50, and 10 μ*M* DAPI. Cells were imaged using a confocal laser scanning microscope.

Immunohistologic studies. Freshly isolated spinal tissues from 3-week-old rats and day 15 embryonic (E15.0) mice were immediately fixed in 4% paraformaldehyde in PBS and were then embedded in paraffin. Transverse and coronal sections were deparaffinized in xylene, rehydrated through a graded ethanol series, and stained with hematoxylin and eosin. For localization of β-catenin, sections were incubated overnight at 4°C with anti–β-catenin antibody (Cell Signaling Technology) in 2% bovine serum albumin (BSA) in PBS at a 1:200 dilution. After thoroughly washing the sections, the bound primary antibody was incubated for 10 minutes at room temperature with a biotinylated universal secondary antibody at a dilution of 1:20 (Vector Laboratories). Sections were incubated with a streptavidin/peroxidase complex for 5 minutes, washed with PBS, and color was developed using 3′-3-diaminobenzidine (Vector Stain Universal Quick Kit; Vector Laboratories).

MTT assay. Effects on cellular proliferation were also measured with a modified MTT assay, based on the ability of live cells to utilize thiazolyl blue and convert it to the water-insoluble dark blue formazan stain. Exponentially growing NP cells were seeded into a 24-well plate at 1.5×10^4 cells/well. After LiCl stimulation (1–20 m*M* for 24–72 hours), cells were treated with MTT (5 gm/liter; Sigma-Aldrich) for 2 hours at 37°C, and then DMSO was added to each well, and the reaction was incubated for 30 minutes. Subsequently, the cells were transferred to a 96-well plate, and a microtiter plate reader (Pharmacia) was used to quantify the absorbance at 590 nm. All experiments were performed 3 times, each in triplicate.

Caspase assays. NP cells were seeded on 96-well plates at a density of 1×10^4 cells/well. NP cells without LiCl treatment were included as controls. After 24 hours of treatment, the cell proliferation and activity of caspases 3/7, 8, and 9 in 2 separate microtiter plates were examined using the CellTiter-Glo luminescent cell viability assay (Promega), a cell viability assay based on the quantitation of ATP in metabolically active cells, and the Caspase-Glo 3/7, 8, and 9 assay (Promega), a caspase assay that measures the activity of caspases 3/7, 8, and 9. Briefly, the plates containing NP cells were removed from the incubator and allowed to equilibrate to room temperature for 30 minutes. Then, 100 μl of CellTiter-Glo reagent and Caspase-Glo reagent were added to each well, and the plate was gently mixed with a plate shaker at 300–500 revolutions per minute for 30 seconds. The plate was then incubated at room temperature for 2 hours. The luminescence of each sample was measured in a plate-reading luminometer (GloMax 20/20n; Promega). The caspase luminescence was normalized to cell viability luminescence.

Cell cycle analysis. NP and AF cells were grown at 37°C in 24-well plates in a humidified atmosphere containing 5% CO_2. The seeding density was 5×10^4 cells/ml. Flasks were preincubated overnight before the addition of the drug solutions (LiCl) or the control. The cells were incubated for 1 hour with 10 μ*M* 5-bromo-2′-deoxyuridine (BrdU). The cells were stained for intracellular BrdU and Ki-67 using a BrdU Flow kit (Becton Dickinson) according to the manufacturer's protocol. Briefly, NP and AF cells were fixed, permeabilized in BD Cytofix/Cytoperm buffer for 15 minutes on ice, washed with BD Perm/Wash buffer, and then incubated with BD Cytofix/Cytoperm Plus buffer for 10 minutes on ice. Cells were then washed with the BD Perm/Wash buffer, refixed with BD Cytofix/Cytoperm buffer on ice for 5 minutes, and treated for 1 hour at 37°C with DNase I at a concentration of 300 μg/ml. Cells were then stained with fluorescein isothiocyanate–labeled anti-BrdU and allophycocyanin-labeled Ki-67 (Becton Dickinson), diluted in BD Perm/Wash buffer, and incubated for 20 minutes at room temperature. Finally, cells were washed and resuspended in staining buffer. Flow cytometric analysis was performed with a FACSAria cytometer, and the findings were analyzed using the FACSDiva software program (both from Becton Dickinson).

Staining for senescence-associated β-galactosidase (β-gal). We stained NP and AF cells for senescence-associated β-gal activity with the use of a cell senescence histochemical staining kit (catalog no. CS0030; Sigma-Aldrich) according to the manufacturer's protocol. Cells were treated for 24 hours in the presence or absence of 20 m*M* LiCl. For purposes of quantification, a minimum of 100 cells spanning 5 different microscopy fields were scored for staining.

Real-time reverse transcription–polymerase chain reaction (RT-PCR) analysis. NP cells were cultured in 6-cm plates (5×10^5 cells/plate) with or without 20 m*M* LiCl and were transfected with WNT-3a or β-catenin expression vectors. Total RNA was extracted according to the TRIzol RNA isolation protocol (Invitrogen). Before elution from the column, RNA was treated with RNase-free DNase I. Total RNA (100 ng) was used as a template for the real-time RT-PCR analyses. Messenger RNA (mRNA) was quantified using an ABI 7500 Fast Real-Time PCR system (Applied Biosystems). Complementary DNA (cDNA) was synthesized by the reverse transcription of mRNA, as previously described (5). Real-time PCR analyses were performed in duplicate using 96-well plates with Fast SYBR Green Master Mix (Applied Biosystems). GAPDH was used as an endogenous control.

Two microliters of cDNA per sample was used as the template for the real-time PCR; 1 μl of forward primer and 1 μl of reverse primer were added to 20 μl of SYBR Green Master Mix. Reactions were synthesized in a 20-μl reaction volume under the following conditions: initial step at 50°C for 2 minutes, followed by 95°C for 10 minutes, and then 40 cycles at 95°C for 3 seconds (denaturation) and 60°C for 30 seconds (hybridization/elongation). All primers were synthesized by Takara Bio, as follows: β-catenin (AF_121265.1), MMP-2 (NM_031054.2), MMP-3 (NM_133523.1), MMP-7 (NM_012864.2), MMP-9 (NM_031055.1), MMP-10 (NM_133514.1), MMP-13 (NM_133530.1), transforming growth factor β3 (TGFβ3) (NM_013174.1), aggrecan (NM_022190.1), and Col2a1 (NM_012929.1). To normalize each sample, a control gene (GAPDH) was used, and the

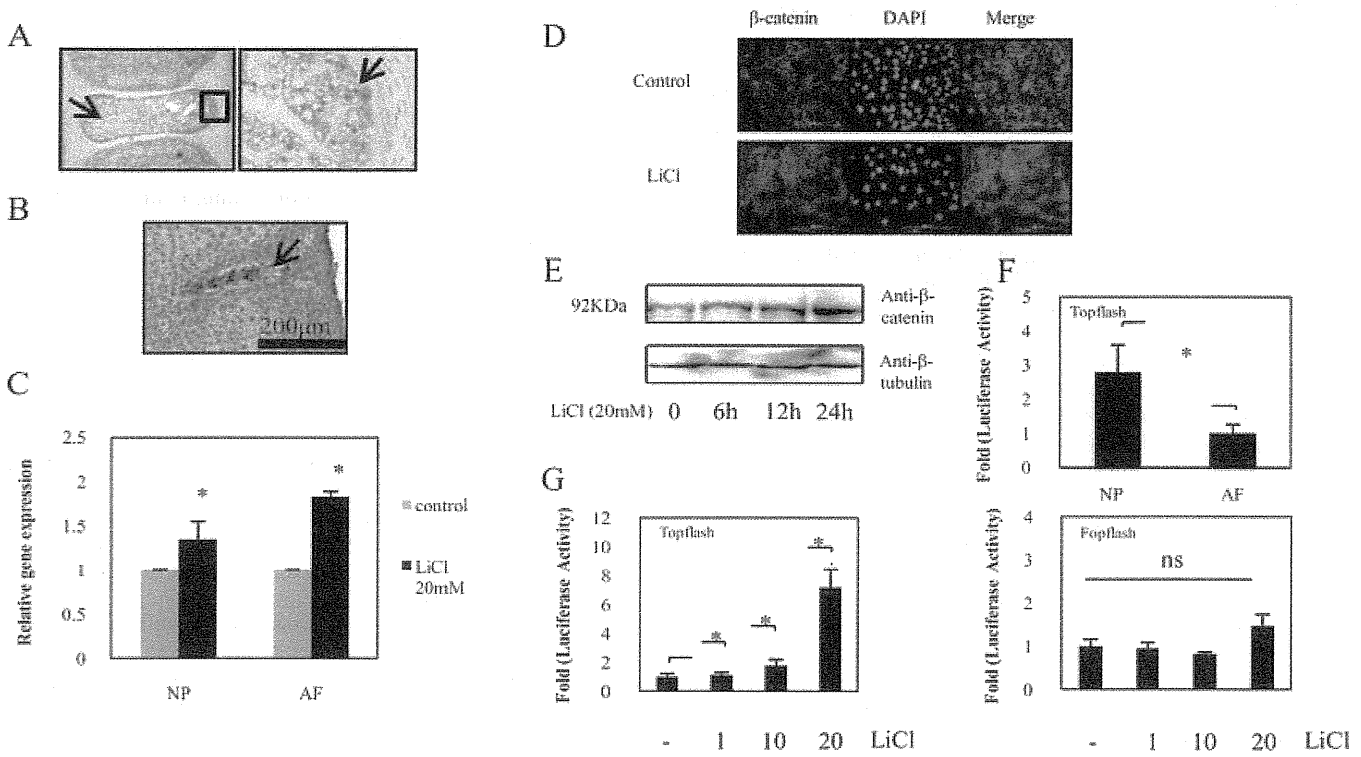

Figure 1. A and **B,** Sagittal sections of an intervertebral disc from a neonatal rat (**A**) and an embryonic mouse (obtained on day 15.0 of embryogenesis) (**B**). Sections were treated with an anti–β-catenin antibody, and counterstained with hematoxylin. Nucleus pulposus (NP) cells expressed β-catenin protein (**arrows**). In **A**, the boxed area in the left panel is shown at higher magnification in the right panel. **C,** Real-time reverse transcription–polymerase chain reaction analysis of β-catenin mRNA levels in NP cells and in anulus fibrosus (AF) cells cultured for 24 hours in the presence or absence of 20 m*M* LiCl. Values are the mean and SD. * = $P < 0.05$ versus controls. **D,** Detection of β-catenin expression by immunofluorescence microscopy. After 24 hours of culture in the presence or absence of 20 m*M* LiCl, NP cells were fixed and stained with an antibody raised against β-catenin as well as with DAPI (to identify healthy nuclei). There was nuclear localization of β-catenin in cells treated with LiCl as compared with the positive control. The merge image represents cells stained with β-catenin and DAPI. Bars = 200 μm (original magnification × 10). **E,** Representative Western blot showing a detectable increase in β-catenin protein levels at 6 hours after treatment with 20 m*M* LiCl. **F,** Basal activities of TOPflash in both NP cells and AF cells were determined by dual luciferase assay. **G,** NP cells were cotransfected with the TOPflash reporter plasmid (left) or with the FOPflash reporter plasmid and pGL4.74 plasmid (right). Values in **F** and **G** are the mean and SD. * = $P < 0.05$. NS = not significant.

arbitrary intensity threshold (C_t) of amplification was computed. The expression scores were obtained by the $\Delta\Delta C_t$ calculation method. Statistical significance was determined with the SPSS version 14.0 software program, using Kruskal-Wallis nonparametric analysis with Mann Whitney U post hoc testing. *P* values less than 0.05 were considered statistically significant.

Microarray analysis. Oligo GEArray Rat TGFβ/BMP Signaling Pathway Microarrays (ORN-035; SABiosciences) were used for expression profiling in conjunction with a TrueLabeling-AMP linear RNA amplification kit, according to the manufacturer's protocols. The expression profiles from the array experiments were analyzed with the GEArray expression analysis software suite (SABiosciences).

Western blot analysis. NP cells were left untreated or were treated with 20 m*M* LiCl for 24 hours. After treatment, NP cells were immediately placed on ice and washed with cold PBS. Proteins were prepared using a CelLytic NuClear extraction kit (Sigma-Aldrich). All wash buffers and the final resuspension buffer included 1× protease inhibitor cocktail (Pierce), NaF (5 m*M*), and Na_3VO_4 (200 m*M*). Nuclear or total cell proteins were resolved on a sodium dodecyl sulfate polyacrylamide gel and were electrotransferred to nitrocellulose membranes (Bio-Rad). The membranes were blocked with 5% BSA in TBST (50 m*M* Tris, pH 7.6, 150 m*M* NaCl, and 0.1% Tween 20) and were incubated overnight at 4°C in 5% BSA in TBST with anti–β-catenin (1:1,000 dilution; Cell Signaling Technology). Immunolabeling was detected with the enhanced chemiluminescent reagent (Amersham Biosciences).

Transfections and dual luciferase assay. One day prior to transfection, NP cells were transferred to 24-well plates at a density of 6×10^4 cells/well. The next day, NP cells were treated with 1, 10, or 20 m*M* LiCl with 900 ng of TOPflash or FOPflash reporter plasmid and 100 ng of the pGL4.74 plasmid to investigate the effects of LiCl on TOPflash and FOPflash

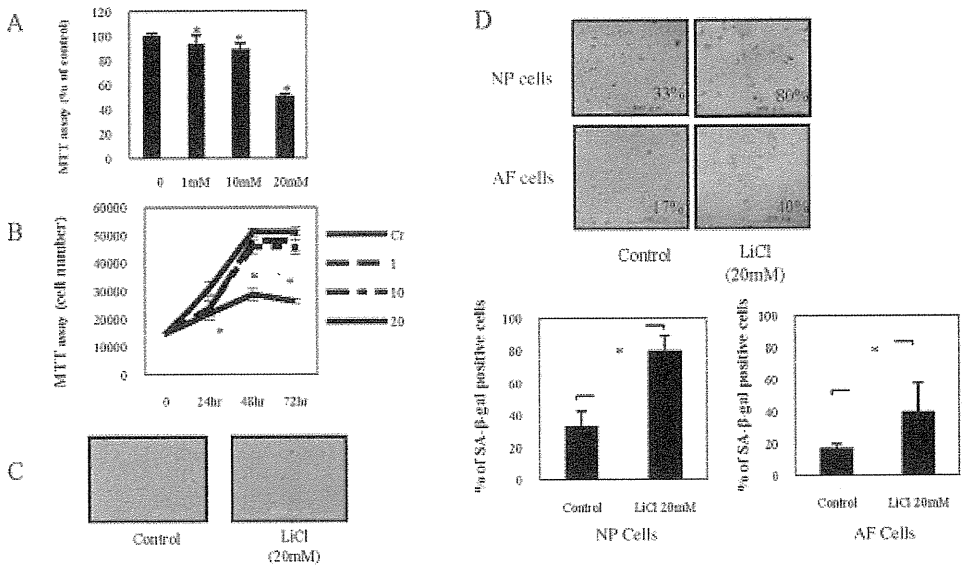

Figure 2. A and **B,** Determination of cell viability in nucleus pulposus (NP) cells. NP cells were pretreated for 48 hours (**A**) or for up to 72 hours (**B**) with various concentrations (1–20 m*M*) of LiCl, and cell viability was determined by MTT assay. Values are the mean and SD. * = $P < 0.05$ versus controls (Cr). **C,** Photomicrographs of NP cells harvested from 12-week-old Sprague-Dawley rats and cultured for 24 hours in the presence or absence of 20 m*M* LiCl. Bars = 500 μm (original magnification × 4). **D,** Photomicrographs showing staining of NP cells and anulus fibrosus (AF) cells for senescence-associated β-galactosidase (SA-β-gal), which was determined as the percentage of positive cells (top). Positive staining for SA-β-gal was detectable for 24 hours after LiCl treatment. Bars = 500 μm (original magnification × 4). SA-β-gal staining in NP (left) and AF (right) cells was also quantified (bottom). A minimum of 100 cells spanning 5 different microscopy fields were scored for staining. Values are the mean and SD. * = $P < 0.05$.

activity. In several experiments, cells were cotransfected with 100–500 ng of WT-β-catenin or the backbone vector with 400 ng of Agg-Luc or Col2-Luc reporter and 100 ng of the pGL4.74 plasmid. Lipofectamine 2000 (Invitrogen) was used as a transfection reagent. For each transfection, plasmids were premixed with the transfection reagent. The following day, the cells were harvested, and a dual luciferase reporter assay system (Promega) was used for sequential measurements of firefly luciferase and *Renilla luciferase* activities. Quantification of luciferase activities and calculation of relative ratios were performed with a TD-20/20 luminometer (Turner Designs). At least 3 independent transfections were performed, and all analyses were performed in triplicate.

Statistical analysis. All measurements were performed in triplicate and were repeated with 2 independent cultures. Data are presented as the mean ± SD. To test for significance, data were analyzed using Student's unpaired *t*-test. *P* values less than 0.05 were considered significant.

RESULTS

Expression of β-catenin in intervertebral disc cells. To investigate the role of WNT/β-catenin signaling in the IVD, we first determined whether rat IVDs express β-catenin. The expression of β-catenin in the neonatal rat (3 weeks of age) and the embryonic mouse (day E15.0) are shown in Figures 1A and B. Immunohistologic analyses revealed β-catenin expression in the NP cells. The majority of the staining was nuclear. However, some staining was present in the cytosol of the NP cells.

We further examined the expression of β-catenin by analyzing β-catenin mRNA expression by real-time PCR. Figure 1C shows that treatment with LiCl for 24 hours resulted in increased β-catenin mRNA levels in both NP cells and AF cells. In addition, we determined the expression levels of β-catenin protein in rat NP cells following treatment with LiCl. As shown in Figures 1D and E, immunofluorescence microscopy and Western blotting with an anti–β-catenin antibody, respectively, demonstrated that LiCl treatment induced β-catenin protein expression in NP cells.

To further evaluate the activation of β-catenin

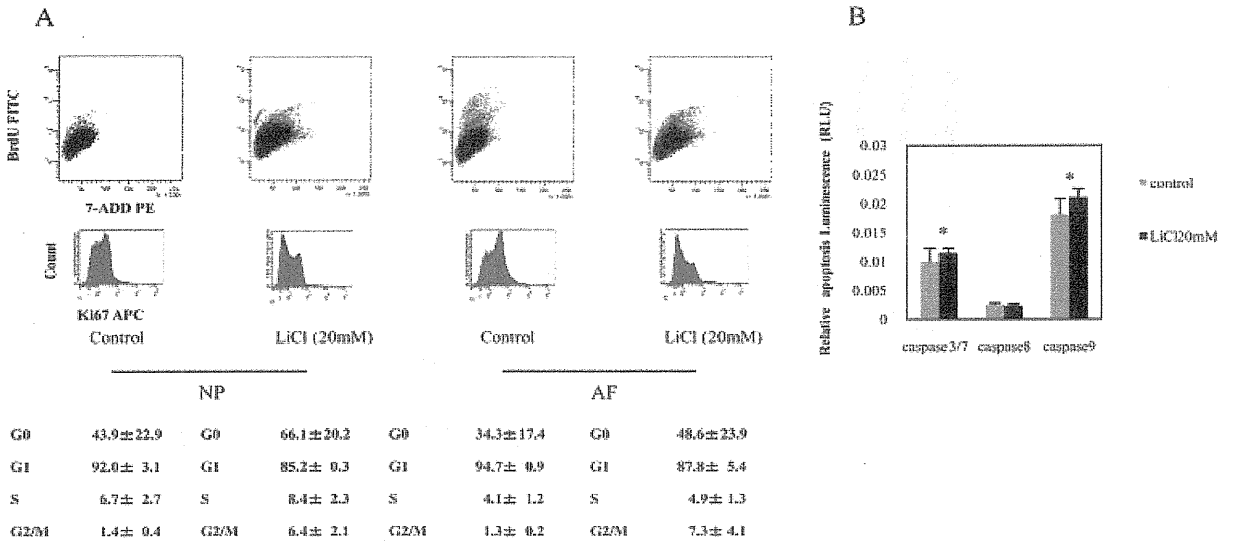

Figure 3. **A,** Cell cycle analysis of nucleus pulposus (NP) and anulus fibrosus (AF) cells. Analysis of the cell cycle was performed using combined 5-bromo-2′-deoxyuridine (BrdU) and 7-aminoactinomycin D (7-AAD) double staining (top row) and allophycocyanin (APC)–labeled Ki-67 staining (bottom row) in NP cells and AF cells treated for 24 hours with 20 m*M* LiCl. The percentages of cells in phases G_1, S, and G_2/M are indicated in each of the flow cytometric dot plots (top). The mean ± SD percentages of Ki-67–negative (G_0) and Ki-67–positive (G_1) cells in the total population were also calculated (bottom). FITC = fluorescein isothiocyanate; PE = phycoerythrin. **B,** Determination of NP cell proliferation and caspase 3/7, 8, and 9 activities. The activity of caspases 3/7, 8, and 9 and NP cell proliferation were quantified in 2 separate microtiter plates using the Caspase-Glo 3/7, 8, and 9 Assay and the CellTiter-Glo Luminescent Cell Viability Assay, respectively. The luminescence values in the caspase assays were normalized to the luminescence in the cell viability assay. Values are the mean and SD of 8 replicates per treatment. * = $P < 0.05$ versus controls.

signaling, we measured the basal activity of the TOPflash reporter in disc cells. Figure 1F shows that NP cells displayed a significantly higher (2.8-fold) basal level of TOPflash activity than did AF cells. We then measured the activity of both TOPflash (containing the wild-type TCF binding sites) and FOPflash (mutant TOPflash) in NP cells after LiCl treatment. Figure 1G shows that there was a dose-dependent increase in the activity of TOPflash upon LiCl stimulation, whereas FOPflash activity was not affected by LiCl treatment.

Induction of cell cycle arrest and apoptosis in intervertebral disc cells by WNT/β-catenin signaling. The effects of WNT/β-catenin signaling on IVDs were examined by MTT assay, cell cycle analysis, and senescence-associated β-gal assay. To determine a suitable concentration, NP cells were treated for 48 hours with various doses of LiCl. After 48 hours, LiCl treatment (20 m*M*) decreased cell viability by 50% (mean ± SD 51.12 ± 1.50%), and this reduction was sustained for up to 72 hours (Figures 2A and B). Therefore, we used a 20 m*M* concentration of LiCl in subsequent experiments in this study. We next examined the morphologic changes in cells after exposure to LiCl (Figure 2C). Treatment with LiCl was shown to decrease the number of NP cells. However, there did not appear to be any marked influence on cell morphology.

To test for cell senescence, we stained cells for the expression of senescence-associated protein β-gal. Figure 2D shows that LiCl treatment for 24 hours increased the average proportion of senescence-associated β-gal–positive NP and AF cells by ~2.4-fold as compared with untreated controls, with a mean ± SD increase of 79.57 ± 9.47% and 32.96 ± 9.58%, respectively, for LiCl and control treatment of NP cells, as compared with 39.59 ± 18.15% and 16.89 ± 2.77%, respectively, for LiCl and control treatment of AF cells ($P < 0.05$). These results indicate that the WNT/β-catenin signaling promotes cellular senescence in both NP and AF cells.

We next determined the cell cycle status of LiCl-treated and control NP and AF cells that had been labeled with BrdU and Ki-67. We considered the G_0 fraction to be cells that did not express Ki-67. A representative fluorescence-activated cell sorter profile of the BrdU-stained and Ki-67–stained cells is shown in Figure 3A. Only 8.4 ± 2.3% (mean ± SD) of LiCl-treated NP cells were in the S phase of the cell cycle, whereas 66.1 ± 20.2% and 85.2 ± 0.3% of these cells were in the G_0 and

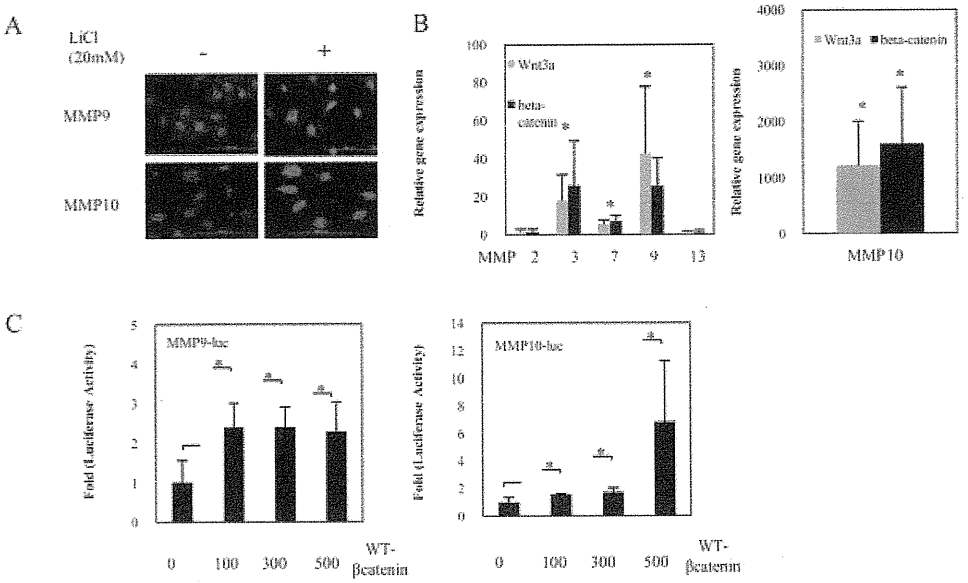

Figure 4. A, Photomicrographs showing matrix metalloproteinase 9 (MMP-9) and MMP-10 expression in nucleus pulposus (NP) cells, as determined by immunofluorescence. NP cells were grown in 96-well plates and exposed to LiCl (20 m*M*) for 24 hours. Cells were stained with the appropriate primary and fluorescence-labeled secondary antibodies. Results are representative of 3 independent experiments per protein. Bars = 200 μm (original magnification × 20). **B,** Effects of the canonical WNT/β-catenin signal in NP cells on the expression of MMP-2, MMP-3, MMP-7, MMP-9, and MMP-13 (left), as well as MMP-10 (right). Relative expression of the MMPs and GAPDH was determined by real-time polymerase chain reaction analysis, quantified, and normalized to the expression in untreated cells, which was arbitrarily set at 1.0. Values are the mean and SD. * = $P < 0.05$ versus controls. **C,** Expression of MMP-9 (left) and MMP-10 (right) in NP cells cotransfected with WT-β-catenin expression plasmid. Levels of MMPs 9 and 10 expression were determined in NP cells cotransfected with MMP-9-Luc (400 ng) or MMP-10-Luc (400 ng) and an increasing concentration of the WT-β-catenin expression plasmid (100–500 ng). Values are the mean and SD. * = $P < 0.05$.

G_1 phases, respectively. In contrast, 6.7 ± 2.7%, 43.9 ± 22.9%, and 92.0 ± 3.1% of control NP cells were in the S, G_0, and G_1 phases, respectively. The number of cells in the G_2/M phase was significantly increased in the presence of LiCl treatment. Similar results were obtained for AF cells.

We assessed the effect of WNT/β-catenin signaling on caspase activation (caspases 3/7, 8 and 9) in NP cells by treating the NP cells with LiCl for 24 hours. We found that the activities of caspases 3/7 and 9 were statistically increased compared with untreated cells, whereas caspase 8 was not activated in response to LiCl treatment (Figure 3B).

Induction of mRNA and protein expression of MMPs in intervertebral disc cells by WNT/β-catenin signaling. To obtain direct evidence that WNT/β-catenin signaling can trigger extracellular matrix degradation and induce the expression of MMPs, we treated NP cells with LiCl and measured MMP expression. Figure 4A shows that LiCl treatment resulted in an increase in MMP-9 and MMP-10 protein expression, as assessed by immunofluorescence microscopy. To investigate the intracellular signaling pathways involved in WNT-3a–induced and β-catenin–induced MMP production in NP cells, NP cells were transiently cotransfected with plasmids encoding WNT-3a or β-catenin. MMP gene expression was significantly increased upon WNT-3a or β-catenin cotransfection. Interestingly, MMP-10 gene expression was much higher as compared with untreated cells (Figure 4B). When NP cells were cotransfected with a WT-β-catenin expression plasmid, there was a significant increase in both MMP-9 and MMP-10 reporter activity (Figure 4C).

Involvement of WNT and TGFβ signaling cross-talk in matrix synthesis. To further investigate the possible mechanisms of WNT/β-catenin signaling in NP cells, we next examined the effect of WNT/β-catenin treatment on aggrecan and type II collagen promoter

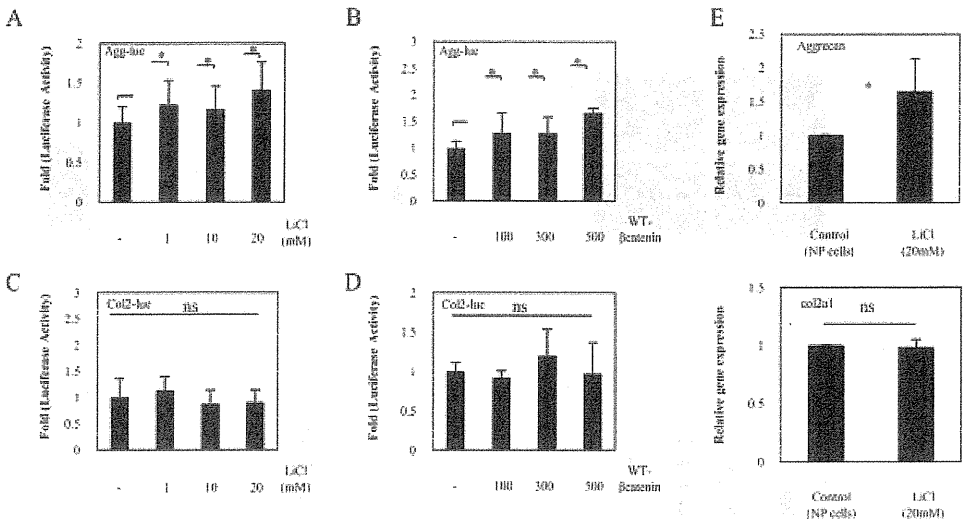

Figure 5. Expression of aggrecan and type II collagen in rat nucleus pulposus (NP) cells. **A–D,** Aggrecan reporter plasmid (**A** and **B**) or type II collagen reporter plasmid (**C** and **D**) was transfected into rat NP cells with the pGL4.74 vector. Cells were then stimulated for 24 hours with increasing concentrations of LiCl (**A** and **C**) or were cotransfected with 400 ng of aggrecan or type II collagen reporter plasmid and an increasing concentration of a WT-β-catenin expression plasmid (**B** and **D**), and reporter activity was measured. **E,** Relative expression of the aggrecan mRNA (top) and Col2a1 mRNA (bottom) was determined by real-time polymerase chain reaction analysis. NP cells were left untreated or were treated with LiCl, and the levels of aggrecan, Col2a1, and GAPDH expression were quantified and normalized to the expression in untreated cells, which was arbitrarily set at 1.0. Values in **A–E** are the mean and SD of 3 independent transfections. * = $P < 0.05$. NS = not significant.

activity in NP cells. When transfected NP cells were treated with LiCl or were cotransfected with a WT-β-catenin expression plasmid, there was a very minimal, but statistically significant, increase in aggrecan reporter activity, whereas type II collagen reporter activity did not increase (Figures 5A–D).

In addition, to investigate the effects of the WNT/β-catenin pathway on the expression of aggrecan gene and type II collagen gene (Col2a1), we analyzed aggrecan and Col2a1 mRNA expression by real-time PCR. As shown in Figure 5E, treatment with 20 m*M* LiCl for 24 hours induced a significant increase in aggrecan mRNA levels in NP cells, whereas Col2a1 mRNA was not affected by LiCl treatment. These data were similar to those in the reporter assay analyses.

We then used TGFβ/BMP signaling pathway microarrays to profile genes regulated by LiCl in rat NP cells. As shown in Figure 6A, LiCl treatment induced an increase in the expression of genes associated with IVD degeneration, such as Col1a1, Col3a1, and TGFβ3. However, Col1a2 gene levels did not change with LiCl treatment (Figure 6A). These data were similar to the results obtained by real-time PCR (data not shown). LiCl-treated NP cells showed a 6.8-fold increase in TGFβ3 mRNA expression (Figure 6B).

DISCUSSION

Recent studies have revealed an important role of the WNT/β-catenin signaling pathway in the pathogenesis of osteoarthritis. However, it is not known whether this signaling pathway is involved in the development of degenerative disc disease. The aim of the present study was to elucidate the role of WNT/β-catenin signaling in IVD cells and in extracellular matrix homeostasis. Our studies demonstrated that WNT/β-catenin signaling accelerates the senescence of NP cells, whereas prolonged activation leads to compromised cell survival due to the induction of cell apoptosis. Importantly, our studies showed that WNT/β-catenin signaling in NP cells induces the expression of MMPs that are involved in the breakdown of extracellular matrix and the progression of disc disease.

In the WNT-3a–knockout mouse, formation of the dorsal mesoblast does not progress appropriately, leading to a loss of the posterior somites and abnormal

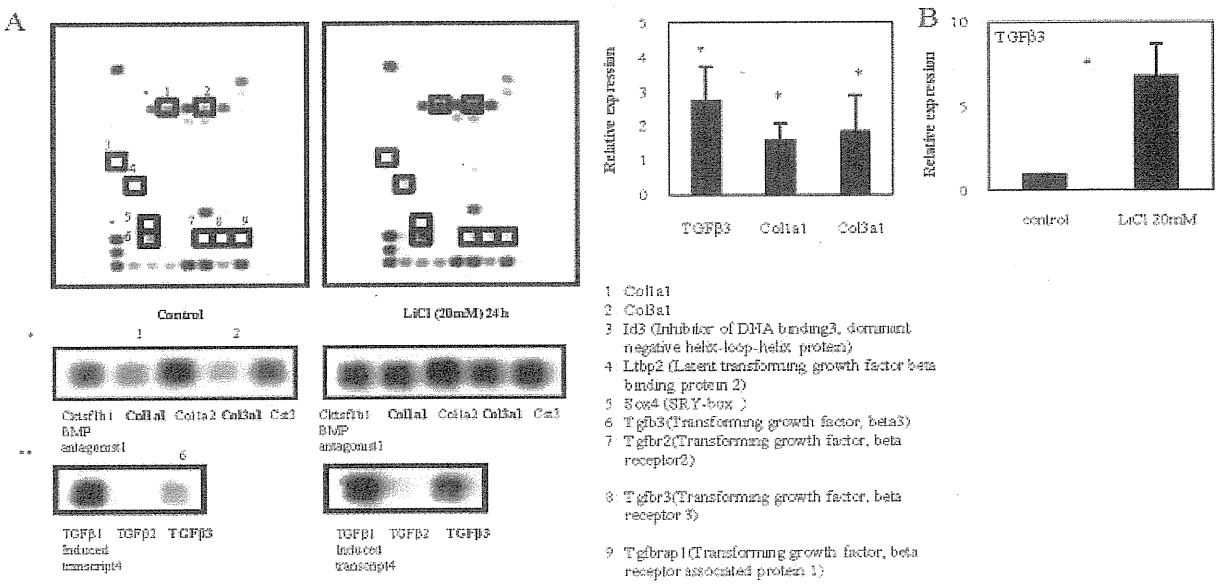

Figure 6. A, Profiling of genes regulated by transforming growth factor β (TGFβ)/bone morphogenetic protein (BMP) signaling in nucleus pulposus (NP) cells. Representative Oligo GEArray profiling results are shown. The intensity of several spots was up-regulated or down-regulated after 24 hours of treatment of NP cells with LiCl (20 m*M*) (right) as compared with controls (left). Regions containing Col1a1, Col3a1, and TGFβ3 are shown at higher magnification in the middle and bottom panels, and demonstrate that the intensity of these spots was markedly increased in the LiCl-treated cells. Band intensities were quantified by densitometry and normalized to control (without treatment) gene levels using CS Analyzer software (version 2.01; Atto). Spots of interest are numbered in the control array and are enclosed in boxes in both the control and the LiCl treatment arrays; the numbers are defined at bottom right. **B,** Relative expression of TGFβ3, Col1a1, and Col3a1 (left) and TGFβ3 following LiCl treatment (right) in NP cells, as determined by real-time polymerase chain reaction analysis. Levels of TGFβ3, Col1a1, Col3a1, and GAPDH expression were quantified and normalized to the expression in untreated cells, which was arbitrarily set at 1.0. TGFβ3 gene expression was significantly increased after 24 hours of treatment of NP cells with LiCl (20 m*M*), with 6.8-fold higher levels than in untreated control cells. Values are the mean and SD. $* = P < 0.05$ versus control.

formation of the notochord and neural tube, which suggests that this signaling pathway is required in the formation of the axial skeleton. Our analysis of β-catenin expression revealed a robust level of expression in notochord cells during embryonic development. A similar expression pattern was observed in the mature rat discs, suggesting that basal levels of WNT/β-catenin signaling may be required for normal functioning of NP cells.

The disappearance of notochord cells correlated with early degenerative changes in the IVD. In humans, the notochord cells typically disappear by 10 years of age, at about the time morphologic signs of degeneration can be seen (31). However, in some species, the notochord cells may disappear very early in life or may persist throughout the life of the animal. Aguiar et al (32) reported that one possible mechanism for the decrease in proteoglycan synthesis is the loss of notochord cells from the surrounding tissue (32). However, the precise mechanisms responsible for the pivotal morphologic changes in notochord cells and their relocation to the NP of the IVD are largely unknown. Ukita et al (33) reported that WNT/β-catenin signaling maintains the notochord fate for progenitor cells and supports the posterior extension of the notochord.

In order to investigate the role of the WNT/β-catenin signaling in disc cells, we first investigated if activation of this pathway modulated cell proliferation. The results of the MTT assay indicated that cell proliferation was significantly slowed by the addition of LiCl, a known activator of WNT/β-catenin signaling. These findings were further validated by the cell cycle analysis, which revealed an LiCl-induced cell cycle arrest in G_2/M phase. Moreover, cell cycle arrest was accompanied by an increase in the levels of senescence-associated β-gal.

The study of cellular senescence of disc cells is a relatively new area of research. Several groups of investigators have demonstrated increased staining for senescence-associated β-gal in cells from degenerated discs as compared with normal disc tissue (34–37).

Although our experiments did not yet determine the identity of the WNT ligand that may initiate these changes, it is clear that increased accumulation of nuclear β-catenin is linked to senescence of disc cells. We observed that cellular senescence was followed by the induction of apoptosis, as confirmed by activation of caspase 9 as well as activation of caspases 3 and 7. Interestingly, activation of caspase 9 suggests mitochondrial involvement in this process. These results suggest that a high level of nuclear β-catenin probably promote cellular changes that are characteristic of early disc degeneration. Future studies will elucidate the molecular mechanisms behind these changes.

Considering the reports of correlations between MMPs, which are catabolic degradation enzymes, and the expression of cellular senescence markers (38), we hypothesized that MMPs may be involved in the increased cellular senescence caused by the activation of the WNT/β-catenin signaling pathway. Our results support this hypothesis, and we confirmed elevated expression of MMPs 3, 7, 9, and 10 following activation of WNT/β-catenin signaling. The expression and activation of these MMPs have been reported to be involved in IVD degeneration.

As a result of assessing the expression of aggrecan and Col2a1, which are major components of the extracellular NP matrix, we found that activation of the WNT/β-catenin signals elevated the reporter activity of aggrecan in a concentration-dependent manner but did not affect the reporter activity of Col2a1. The same results were obtained by real-time PCR analyses. These data demonstrated that the WNT/β-catenin signals are probably not involved in Col2a1 synthesis. Based on the present studies, it is likely that pathologic activation of WNT/β-catenin signaling in disc cells may promote matrix degradation and a subsequent loss of water-binding capacity of the tissue, although the expression of aggrecan was found to be elevated.

We have previously reported that the TGFβ family members are important anabolic factors for proteoglycan synthesis in the disc (39), and we tested our hypothesis that the activation of the WNT/β-catenin signaling may induce the expression of TGFβ family proteins in disc cells. We therefore conducted an assessment using a microarray of the TGFβ family and found that activation of WNT/β-catenin signals significantly elevated the expression of TGFβ3. With regard to TGFβ3, Risbud et al (40) reported that TGFβ3 is important for the homeostasis of disc cells and that TGFβ3 elevated the expression of critical matrix genes by disc cells. It is generally believed that multiple factors are involved in IVD degeneration and that an imbalance between anabolic and catabolic factors induces a decrease in proteoglycan synthesis, thereby promoting disc degeneration.

There are a few limitations with respect to the analyses and data that may affect the accuracy of these results. One limitation of the present study is that we used LiCl to activate WNT signaling (41). Several groups of investigators have used LiCl as an inhibitor of GSK-3β (42–44). Inhibition of GSK-3β leads to the accumulation of β-catenin and the activation of WNT/β-catenin signaling. Since GSK-3β has other functions and since LiCl does not specifically activate the WNT pathway (45), we used WT-β-catenin instead of LiCl, and we also evaluated the effects by a reporter assay and by a cell senescence and cell cycle analysis. The data from these analyses were similar to those obtained after LiCl treatment (data available upon request from the author). Moreover, because we were not able to strictly conclude whether aggrecan synthesis is regulated by 2 opposing processes, called anabolic (TGFβ3) and catabolic (MMP), by WNT/β-catenin signaling, it will be necessary to examine in future studies the effects of WNT-target genes as well as the possible cross-talk between WNT/β-catenin and other signals to confirm the findings of this experiment.

In summary, the findings of the present study suggest the possibility that WNT/β-catenin signals regulate the balance between catabolic factors and anabolic factors in IVD. In addition, WNT/β-catenin signals may have significant involvement in cell proliferation and senescence in IVD cells, perhaps to a greater extent than their involvement in matrix synthesis. Our data support the possibility that as WNT/β-catenin induces cell senescence and MMP expression in disc cells (catabolic arm), it simultaneously promotes the expression of aggrecan through the anabolic factor TGFβ3 (anabolic arm).

ACKNOWLEDGMENT

We thank Dr. Tadayuki Sato for helpful advice and excellent technical assistance.

AUTHOR CONTRIBUTIONS

All authors were involved in drafting the article or revising it critically for important intellectual content, and all authors approved the final version to be published. Dr. Hiyama had full access to all of the data in the study and takes responsibility for the integrity of the data and the accuracy of the data analysis.

Study conception and design. Hiyama, Sakai, Risbud, Tanaka, Arai, Abe, Mochida.

Acquisition of data. Hiyama, Sakai, Risbud, Tanaka, Arai, Abe, Mochida.
Analysis and interpretation of data. Hiyama, Sakai, Risbud, Tanaka, Arai, Abe, Mochida.

REFERENCES

1. Sakai D, Mochida J, Yamamoto Y, Nomura T, Okuma M, Nishimura K, et al. Transplantation of mesenchymal stem cells embedded in Atelocollagen gel to the intervertebral disc: a potential therapeutic model for disc degeneration. Biomaterials 2003;24:3531–41.
2. Masuda K, Oegema T, An H. Growth factors and treatment of intervertebral disc degeneration. Spine 2004;29:2757–69.
3. Tropiano P, Huang RC, Girardi FP, Marnay T. Lumbar disc replacement: preliminary results with ProDisc II after a minimum follow-up period of 1 year. J Spinal Disord Tech 2003;16:362–8.
4. Thompson JP, Oegema TR Jr, Bradford DS. Stimulation of mature canine intervertebral disc by growth factors. Spine 1991; 16:253–60.
5. Hiyama A, Mochida J, Iwashina T, Omi H, Watanabe T, Serigano K, et al. Transplantation of mesenchymal stem cells in a canine disc degeneration model. J Orthop Res 2008;26:589–600.
6. Hiyama A, Mochida J, Iwashina T, Omi H, Watanabe T, Serigano K, et al. Synergistic effect of low-intensity pulsed ultrasound on growth factor stimulation of nucleus pulposus cells. J Orthop Res 2007;25:1574–81.
7. Masuda K, Imai Y, Okuma M, Muehleman C, Nakagawa K, Akeda K, et al. Osteogenic protein-1 injection into a degenerated disc induces the restoration of disc height and structural changes in the rabbit anular puncture model. Spine 2006;31:742–54.
8. Alini M, Li W, Markovic P, Aebi M, Spiro RC, Roughley PJ. The potential and limitations of a cell-seeded collagen/hyaluronan scaffold to engineer an intervertebral disc-like matrix. Spine 2003;28:446–54.
9. Le Maitre CL, Pockert A, Buttle DJ, Freemont AJ, Hoyland JA. Matrix synthesis and degradation in human intervertebral disc degeneration. Biochem Soc Trans 2007:35:652–5.
10. Le Maitre CL, Freemont AJ, Hoyland JA. Human disc degeneration is associated with increased MMP 7 expression. Biotech Histochem 2006;81:125–31.
11. Le Maitre CL, Freemont AJ, Hoyland JA. Localization of degradative enzymes and their inhibitors in the degenerate human intervertebral disc. J Pathol 2004;204:47–54.
12. Haro H, Crawford HC, Fingleton B, MacDougall JR, Shinomiya K, Spengler DM, et al. Matrix metalloproteinase-3-dependent generation of a macrophage chemoattractant in a model of herniated disc resorption. J Clin Invest 2000;105:133–41.
13. Richardson SM, Doyle P, Minogue BM, Gnanalingham K, Hoyland JA. Increased expression of matrix metalloproteinase-10, nerve growth factor and substance P in the painful degenerate intervertebral disc. Arthritis Res Ther 2009;11:R126.
14. Roberts S, Evans H, Trivedi J, Menage J. Histology and pathology of the human intervertebral disc. J Bone Joint Surg Am 2006;88 Suppl 2:10–4.
15. Ben-Porath I, Weinberg RA. The signals and pathways activating cellular senescence. Int J Biochem Cell Biol 2005;37:961–76.
16. Ben-Porath I, Weinberg RA. When cells get stressed: an integrative view of cellular senescence. J Clin Invest 2004;113:8–13.
17. Campisi J. Senescent cells, tumor suppression, and organismal aging: good citizens, bad neighbors. Cell 2005;120:513–22.
18. Hayflick L, Moorhead PS. The serial cultivation of human diploid cell strains. Exp Cell Res 1961;25:585–621.
19. Janzen V, Forkert R, Fleming HE, Saito Y, Waring MT, Dombkowski DM, et al. Stem-cell ageing modified by the cyclin-dependent kinase inhibitor p16INK4a. Nature 2006;443:421–6.
20. Yuasa T, Otani T, Koike T, Iwamoto M, Enomoto-Iwamoto M. Wnt/β-catenin signaling stimulates matrix catabolic genes and activity in articular chondrocytes: its possible role in joint degeneration. Lab Invest 2008;88:264–74.
21. Rudnicki JA, Brown AM. Inhibition of chondrogenesis by Wnt gene expression in vivo and in vitro. Dev Biol 1997;185:104–18.
22. Kawakami Y, Wada N, Nishimatsu SI, Ishikawa T, Noji S, Nohno T. Involvement of Wnt-5a in chondrogenic pattern formation in the chick limb bud. Dev Growth Differ 1999;41:29–40.
23. Gordon MD, Nusse R. Wnt signaling: multiple pathways, multiple receptors, and multiple transcription factors. J Biol Chem 2006; 281:22429–33.
24. Nusse R. Wnts and Hedgehogs: lipid-modified proteins and similarities in signaling mechanisms at the cell surface. Development 2003;130:5297–305.
25. Peifer M, McEwen DG. The ballet of morphogenesis: unveiling the hidden choreographers. Cell 2002;109:271–4.
26. Yamanaka H, Moriguchi T, Masuyama N, Kusakabe M, Hanafusa H, Takada R, et al. JNK functions in the non-canonical Wnt pathway to regulate convergent extension movements in vertebrates. EMBO Rep 2002;3:69–75.
27. Giles RH, van Es JH, Clevers H. Caught up in a Wnt storm: Wnt signaling in cancer. Biochim Biophys Acta 2003;1653:1–24.
28. Tejpar S, Nollet F, Li C, Wunder JS, Michils G, dal Cin P, et al. Predominance of β-catenin mutations and β-catenin dysregulation in sporadic aggressive fibromatosis (desmoid tumor). Oncogene 1999;18:6615–20.
29. Yamada Y, Miyashita T, Savagner P, Horton W, Brown KS, Abramczuk J, et al. Regulation of the collagen II gene in vitro and in transgenic mice. Ann N Y Acad Sci 1990;580:81–7.
30. Reinhold MI, Kapadia RM, Liao Z, Naski MC. The Wnt-inducible transcription factor Twist1 inhibits chondrogenesis. J Biol Chem 2006;281:1381–8.
31. Trout JJ, Buckwalter JA, Moore KC, Landas SK. Ultrastructure of the human intervertebral disc. I. Changes in notochordal cells with age. Tissue Cell 1982;14:359–69.
32. Aguiar DJ, Johnson SL, Oegema TR. Notochordal cells interact with nucleus pulposus cells: regulation of proteoglycan synthesis. Exp Cell Res 1999;246:129–37.
33. Ukita K, Hirahara S, Oshima N, Imuta Y, Yoshimoto A, Jang CW, et al. Wnt signaling maintains the notochord fate for progenitor cells and supports the posterior extension of the notochord. Mech Dev 2009;126:791–803.
34. Takada S, Stark KL, Shea MJ, Vassileva G, McMahon JA, McMahon AP. Wnt-3a regulates somite and tailbud formation in the mouse embryo. Genes Dev 1994;8:174–89.
35. Roberts S, Evans EH, Kletsas D, Jaffray DC, Eisenstein SM. Senescence in human intervertebral discs. Eur Spine J 2006;15: 312–6.
36. Gruber HE, Ingram JA, Norton HJ, Hanley EN Jr. Senescence in cells of the aging and degenerating intervertebral disc: immunolocalization of senescence-associated β-galactosidase in human and sand rat discs. Spine 2007;32:321–7.
37. Le Maitre CL, Freemont AJ, Hoyland JA. Accelerated cellular senescence in degenerate intervertebral discs: a possible role in the pathogenesis of intervertebral disc degeneration. Arthritis Res Ther 2007;9:R45.
38. Struewing IT, Durham SN, Barnett CD, Mao CD. Enhanced endothelial cell senescence by lithium-induced matrix metalloproteinase-1 expression. J Biol Chem 2009;284:17595–606.
39. Hiyama A, Mochida J, Omi H, Serigano K, Sakai D. Cross talk between Smad transcription factors and TNF-α in intervertebral disc degeneration. Biochem Biophys Res Commun 2008;369: 679–85.
40. Risbud MV, Di Martino A, Guttapalli A, Seghatoleslami R, Denaro V, Vaccaro AR, et al. Toward an optimum system for

intervertebral disc organ culture: TGF-β3 enhances nucleus pulposus and anulus fibrosus survival and function through modulation of TGF-β-R expression and ERK signaling. Spine 2006;31: 884–90.
41. Klein PS, Melton DA. A molecular mechanism for the effect of lithium on development. Proc Natl Acad Sci U S A 1996;93: 8455–9.
42. Berridge MJ, Downes CP, Hanley MR. Neural and developmental actions of lithium: a unifying hypothesis. Cell 1989;59:411–9.
43. Stambolic V, Ruel L, Woodgett JR. Lithium inhibits glycogen synthase kinase-3 activity and mimics wingless signalling in intact cells. Curr Biol 1996;6:1664–8.
44. Spencer GJ, Utting JC, Etheridge SL, Arnett TR, Genever PG. Wnt signalling in osteoblasts regulates expression of the receptor activator of NF-κB ligand and inhibits osteoclastogenesis in vitro. J Cell Sci 2006;119:1283–96.
45. Crabtree GR, Olson EN. NFAT signaling: choreographing the social lives of cells. Cell 2002;109 Suppl:S67–79.